	H_P	H_M	H_{PT}	H_C
λ (mm)	14.24	12.74	15.52	11.59
κ (-)	0.83	0.9	0.98	1.08

Table 4.5: Scale (λ) and shape (κ) parameter of Weibull distributions fitting the left-censored observations of each variable.

scribing H_P is characterized by a slightly less heavy tail than that of observations which, however, all fall within the sampling uncertainty interval. As for H_M and H_{PT}, Figure 4.14(b) and (c) show that the related Weibull distributions have a little heavier tail than the observations but, also for these variables, all ordinary events used for the fit are within the related sampling uncertainty interval with the exception of few H_M observations with values around 30 mm. As regards H_C, the highest observations tend to deviate downward with respect to the bisector and some of them are outside the sampling uncertainty interval (Figure 4.14(d)). This means that, for this variable, the Weibull distribution represents a tail that is heavier than the observations one. The fraction of observations used for the fit that is outside the sampling uncertainty interval, on the other hand, is around 3%, namely much less than 10%.

Therefore, consistently with the previous studies cited in Section 4.2.4, the Weibull distribution is deemed suitable for representing the right tail of all the investigated variables.

The parameters of each fitted distribution are reported in Table 4.5 and the resulting CDF, along with the related 90% confidence intervals, are shown in Figure 4.15. Coherently with the related observations behaviour, G_P and G_C are the CDF with the lowest and highest shape parameter, namely with the heaviest and lightest tail, respectively. All the 90% confidence intervals have a bandwidth that varies between about 11% and 30% of the related CDF values, considering non-exceedance probabilities in the range $[0.75, 0.9999]$.

4.5.3 Dependence structure modelling

4.5.3.1 Fitted vine copula

The application of the procedure described in Section 4.4.3 to the pseudo-observations of the investigated variables results in a four-dimensional D-vine copula. The structure of the resulting D-vine copula is shown in Figure 4.16 and, according to it, the copula density c is estimated with the following

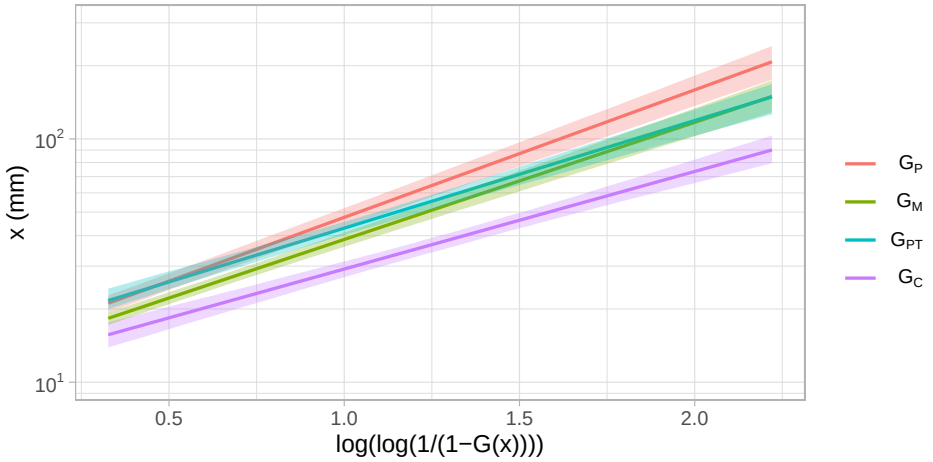

Figure 4.15: Fitted Weibull CDF for each investigated variable along with the related 90% confidence intervals (shaded areas). Each CDF is represented starting from the related 75th percentile, namely the quantile associated to the non-exceedance probability used as threshold to left censor the observations.

factorisation:

$$\begin{aligned} c(u,v,w,z) =& c_{UV}(u,v)\cdot c_{VW}(v,w)\cdot c_{WZ}(w,z)\cdot \\ & c_{UW|V}(F_{U|V}(u|v),F_{W|V}(w|v))\cdot \\ & c_{VZ|W}(F_{W|V}(w|v),F_{W|Z}(w|z))\cdot \\ & c_{UZ|VW}(F_{U|VW}(u|vw),F_{Z|VW}(z|vw)) \end{aligned} \tag{4.77}$$

The families of the six (conditional) copulas along with the related parameter(s) and theoretical Kendall's tau are reported in Table 4.6 and the overall AIC is equal to -1569.9. Considering the first tree, the dependence struc-

	Family	Parameter(s)	τ_C
C_{UV}	BB8	$\theta_1 = 4.76,\ \theta_2 = 0.8$	0.52
C_{VW}	Gumbel	$\theta = 2.32$	0.57
C_{WZ}	BB8	$\theta_1 = 4.56,\ \theta_2 = 0.87$	0.56
$C_{UW\|V}$	t	$\theta_1 = 0.35,\ \theta_2 = 7.48$	0.23
$C_{VZ\|W}$	t	$\theta_1 = 0.32,\ \theta_2 = 5.14$	0.21
$C_{UZ\|VW}$	t	$\theta_1 = 0.11,\ \theta_2 = 9.17$	0.07

Table 4.6: Family, related parameter(s) and theoretical Kendall's tau τ_C of the six (conditional) bivariate copulas present in the obtained D-vine. The related D-vine trees are shown in Figure 4.16.

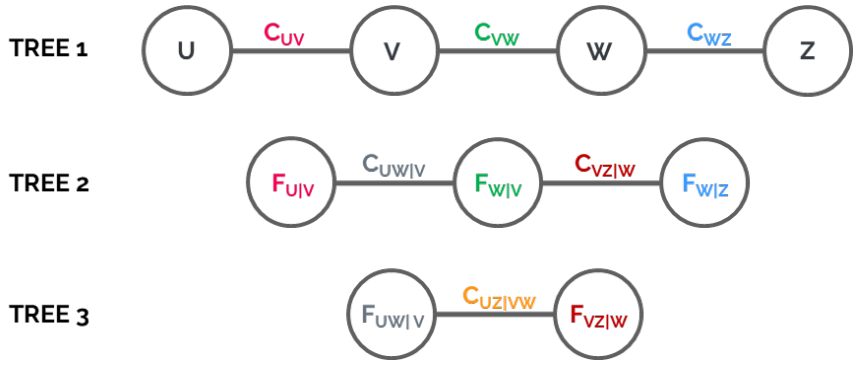

Figure 4.16: Resulting four-dimensional D-vine copula fitting the pseudo-observations dependence structure.

tures between the variable pairs (U, V) and (W, Z) are reproduced by a BB8 copula while a Gumbel copula describes the dependence structure between V and W. Regarding T_2 and T_3, the dependence structures between all the present conditional variables pairs are reproduced by t copulas. The related theoretical Kendall's tau decrease moving from T_1 to T_3 ranging between 0.57 and 0.07. As evident, the overall concordance measure in the last tree is very low but, according to the independence test, it is statistically significant with p-value= 0.03. As a result, a t copula is considered rather than an independence copula.

4.5.3.2 Validation of the fitted D-vine copula

As described in Section 4.4.3, the adequacy of the obtained D-vine copula is assessed considering some copula-related quantities, i.e the Kendall function, λ-function, Kendall tau and TCF, and evaluating how well the empirical values of these quantities are reproduced by each (conditional) bivariate copula and overall D-vine copula.

As regard the pair-copulas, the empirical and theoretical Kendall functions and the corresponding λ-functions for each (conditional) bivariate copula are shown in Figure 4.17 and 4.18, respectively, along with the related 90% sampling uncertainty intervals. It is worth noting that the theoretical Kendall function and λ-function of the t copulas, present in T_2 and T_3, are estimated by simulation. For a graphical comparison, also the Kendall function and λ-function of the comonotonicity and independence copula, computed using Eq. 4.11, 4.12 and 4.15, are represented in all graphs. Coherently to the theoretical Kendall's tau, also from Figure 4.17 and 4.18 it is possible to notice how the overall dependence between the (conditional)

variables pairs becomes weaker moving from T_1 to T_3: both the empirical and theoretical Kendall function and λ-function gradually become closer and closer to the independence copula ones until almost reaching it in T_3.

The obtained $RMSE$ related to the Kendall function and λ-function for each (conditional) bivariate copula are reported in Table 4.7.

As evident from Figure 4.17(a) and 4.18(a), the BB8 copula, that models the dependence between variables U and V, reproduces satisfactorily the empirical Kendall function and λ-function, mainly for high and low values of t. For $t \in [0.1, 0.75]$, the theoretical functions slightly overestimate or underestimate the related empirical values. However, most empirical points, with the exception of a some estimates around $t = 0.65$ and $t = 0.15$, are inside the 90% sampling uncertainty intervals and the resulting $NRMSE$ is equal to 0.096. A satisfactorily reproduction of the empirical Kendall function and λ-function is also performed by the Gumbel copula for the variables pair (V, W) (Figure 4.17(b) and 4.18(b)): for all values of t, the empirical estimates and the theoretical functions are very close, substantially all the empirical points are inside the 90% sampling uncertainty intervals and the $NRMSE$ is 0.08. The last bivariate copula of the first tree reproduces the dependence structure between the variables W and Z in a very similar way to the first BB8 copula for the related variables (Figure 4.17(c) and 4.18(c)): the best agreement between empirical estimates and theoretical functions is for high and low values of t while the worst one is for intermediate values. Nevertheless, also in this case, all empirical points, but few around $t = 0.5$, fall within the 90% sampling uncertainty intervals and the resulting $NRMSE$ is equal to 0.091. A slightly underestimate of the empirical estimates, for intermediate values of t, characterizes the theoretical Kendall function and λ-function of the t copula that reproduces the dependence between the conditional variables $F_{U|V}$ and $F_{W|V}$ (Figure 4.17(d) and 4.18(d)). This copula reproduces satisfactorily the empirical Kendall function and λ-function related to the highest values of t and only some empirical estimates with $t \in (0, 0.1]$ are outside of the 90% sampling uncertainty intervals. The resulting $NRMSE$ is 0.06. A satisfactory agreement can be noted also between the theoretical and empirical Kendall function and λ-functions of the t copula describing the dependence between the conditional variables $F_{V|W}$ and $F_{Z|W}$ for $t \in [0.6, 1)$ (Figure 4.17(e) and 4.18(e)). Instead, for $t \in [0.1, 0.6]$, the theoretical functions slightly overestimate or underestimate the empirical values. Nevertheless, all empirical points, but few with $t \in (0, 0.1]$, are within the 90% sampling uncertainty intervals and the related $NRMSE$ is equal to 0.07. As regard the t copula of T_3, the theoretical and empirical Kendall function and λ-function are always very

close (Figure 4.17(f) and 4.18(f)). The 90% sampling uncertainty intervals contain all empirical points and it is interesting to note that their lower bounds approximately overlap the Kendall function and λ-function of the independence copula. The $NRMSE$ of this reproduction is equal to 0.032.

As regards the theoretical and empirical TCF, the results for each (conditional) bivariate copula are shown in Figure 4.19 along with the 90% sampling uncertainty interval and the independence and comonotonicity copula TCF. Coherently to the previously described results, also these plots highlight the weakening of the overall dependence structure between the (conditional) variables pairs, moving from the first to the last tree.

The obtained $RMSE$ related to the TCF of each (conditional) bivariate copula are reported in Table 4.7.

As evident from Figure 4.19, an upper tail dependence which does not converge to 0 when t tends to 1^- characterizes the Gumbel copula and the t copulas. Instead, the BB8 copulas slowly converge to 0 when t tends to 1^- and the convergence is slower the closer θ_2 is to 1. Moreover, the BB8 copulas and the Gumbel copula are characterized by an asymmetrical TCF while the t copulas by a symmetrical TCF. In general, the TCF asymmetry of a BB8 copula and a Gumbel copula is more marked the greater the θ_1 and θ are, respectively.

As shown in Figure 4.19(a), the behavior of the pseudo-observations of the variables U and V close to the upper right corner of $\mathbb{I}^2$ is satisfactorily reproduced by the BB8 copula, given the proximity between the theoretical and empirical TCF for $t \in [0.8, 1)$. The worst fit subsists for $t \in [0.15, 0.25]$ where the empirical estimates are also outside of the 90% sampling uncertainty interval. Instead, all the empirical estimates of the upper tail are within the 90% sampling uncertainty interval. The $NRMSE$ of this reproduction is equal to 0.082. The strong upper tail dependence between V and W is satisfactory modelled by the Gumbel copula whose theoretical function captures its average trend (Figure 4.19(b)). Also the empirical lower tail is well reproduced: only a few empirical estimates for $t \in [0.05, 0.1]$ are outside of the 90% sampling uncertainty interval. The resulting $NRMSE$ is equal to 0.094. It is worth noting that the spikes that characterize the TCF_n are also present in the limits of the 90% sampling uncertainty interval that has a very high bandwidth for values of t close to 0^+ and 1^-. A satisfactorily reproduction is also performed by the BB8 copula for the tail dependence between the variables W and Z (Figure 4.19(c)): overall, the TCF_n trend is captured, only few empirical estimates around $t = 0.1$ and $t = 0.6$ are not within the 90% sampling uncertainty interval and $NRMSE = 0.076$. As re-

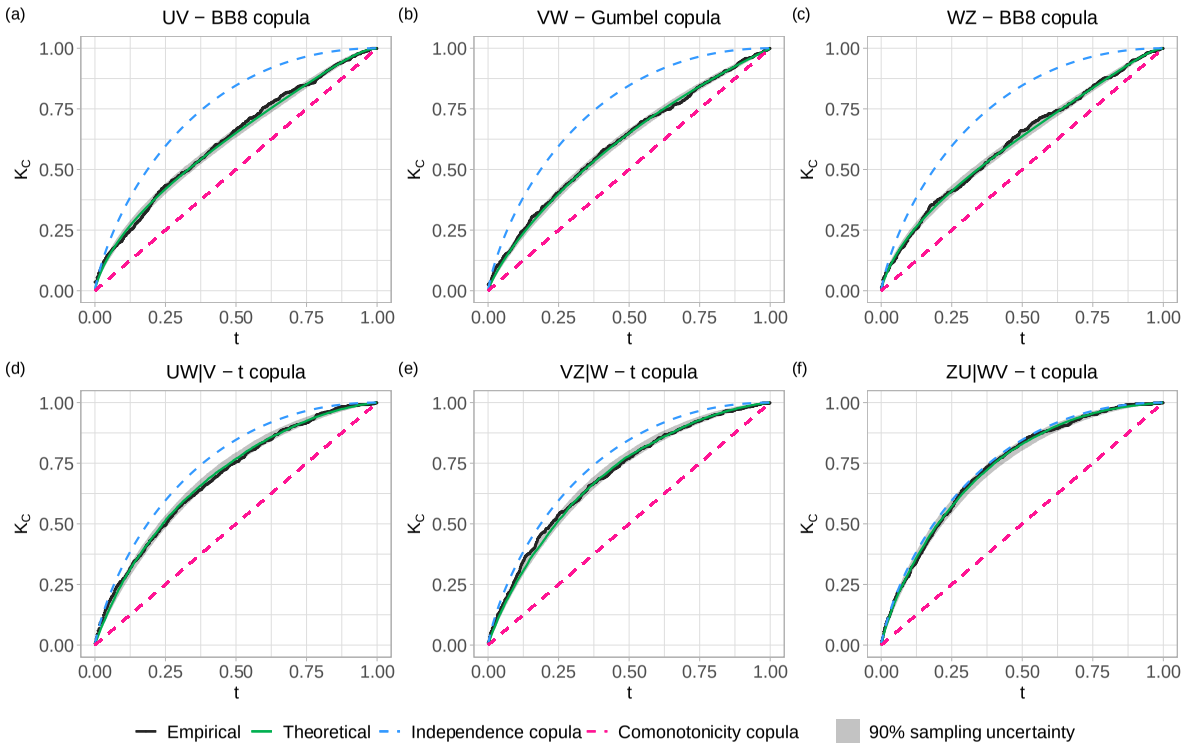

Figure 4.17: Empirical (black line with dots) and theoretical (green line) Kendall function of each (conditional) bivariate copula of the obtained D-vine copula along with the related 90% sampling uncertainty interval. The theoretical Kendall functions of the independence (dashed blue line) and comonotonicity (dashed magenta line) copulas are also reported in each graph. The theoretical Kendall functions of t copulas are estimated by simulation. The (conditional) copula to which each graph refers is indicated in the title by reporting the related subscript.

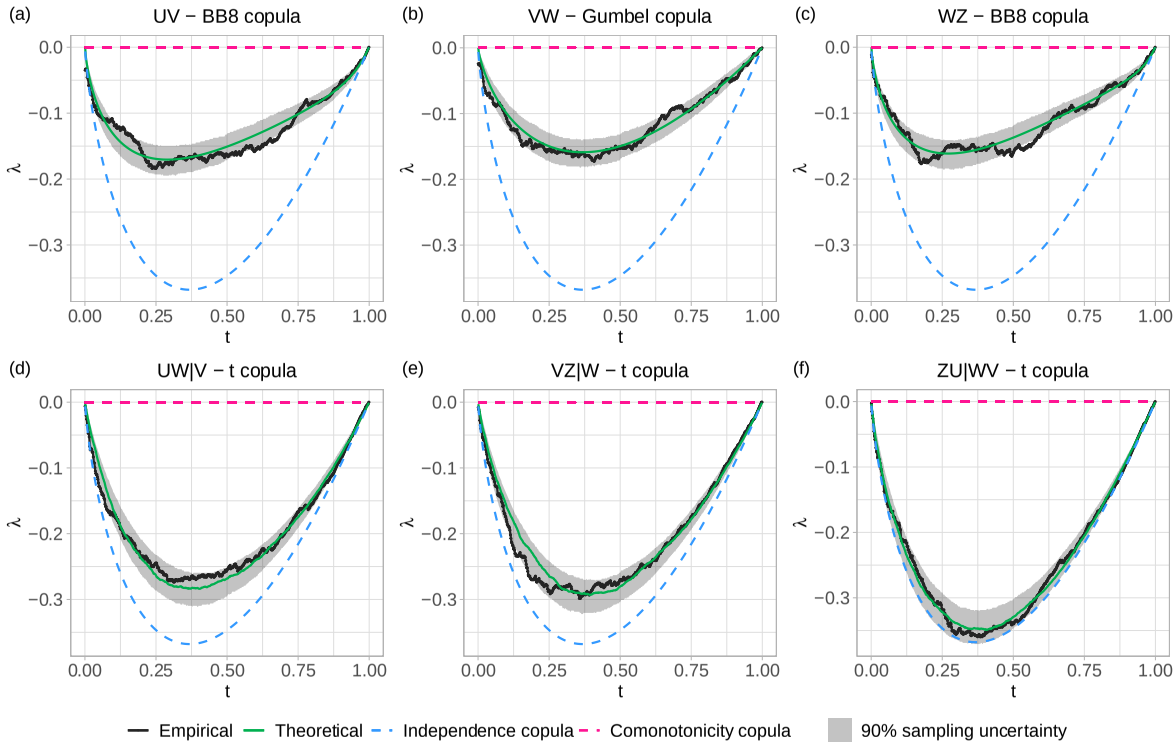

Figure 4.18: Empirical (black line with dots) and theoretical (green line) λ-function of each (conditional) bivariate copula of the obtained D-vine copula along with the related 90% sampling uncertainty interval. The theoretical λ-functions of the independence (dashed blue line) and comonotonicity (dashed magenta line) copulas are also reported in each graph. The theoretical λ-functions of t copulas are estimated by simulation. The (conditional) copula to which each graph refers is indicated in the title by reporting the related subscript.

gards T_2, the t copula that models the dependence between the conditional variables $F_{U|V}$ and $F_{W|V}$ provides a theoretical TCF that reproduces better the empirical trend of the upper tail rather than the lower one (Figure 4.19(d)). For $t \in (0, 0.2]$, the empirical values are overestimated by the theoretical ones and some of them are outside of the 90% sampling uncertainty interval. Conversely, all the empirical points for $t \in [0.52, 1)$ are within the uncertainty interval. The overall $NRMSE$ is equal to 0.156. As regard the t copula that models the dependence between the conditional variables pairs $F_{V|W}$ and $F_{Z|W}$, the theoretical TCF accurately reproduces both the empirical upper and lower tail dependence trends, with only a slight overestimate of the empirical values for $t \in [0.05, 0.4]$ (Figure 4.19(e)). Moreover, all the empirical points are within the 90% sampling uncertainty interval and the resulting $NRMSE$ is equal to 0.138. Also the theoretical TCF of the t copula of T_3 satisfactorily reproduces the related TCF_n for all values of t, only few empirical estimates around $t = 0.5$ are outside of the 90% sampling uncertainty interval (Figure 4.19(f)) and $NRMSE = 0.086$. Coherently to the related results in terms of Kendall function and λ-function, the lower bound of the sampling uncertainty interval of this copula approximately overlap the independence copula TCF.

The last copula-related quantity used to validate each pair-copula of the obtained D-vine is Kendall's tau. The empirical and theoretical Kendall's tau along with the 90% sampling uncertainty interval of each (conditional) bivariate copula are shown in Figure 4.20 while the obtained NAD are reported in Table 4.7. As evident form Figure 4.20, for all copulas, the theoretical value is very closed to the empirical one that is also always inside the sampling uncertainty interval. The overall empirical dependence between the pseudo-observations of the variables U and V is the one reproduced in a more accurate way, with a $NAD = 0.006$, while the worst reproduced is the one among the pseudo-observations of the conditional variables $F_{U|VW}$ and $F_{Z|VW}$ with a $NAD = 0.11$.

Therefore, all the copula-related quantities, considered for the validation of the pair-copulas of the obtained D-vine, highlight a satisfactory reproduction of the empirical values by the theoretical ones. As evident from Table 4.7, the maximum $NRMSE$ is equal to 0.096 and 0.156 for Kendall function and λ-function and TCF, respectively, while in terms of Kendall's tau, the maximum NAD is equal to 0.11. These values can be considered satisfactory. Moreover, in terms of Kendall function, λ-function and TCF, the best results are obtained for high values of t, namely for the copula probability levels of interest for the following scenarios estimate. The pair-copulas adequacy is further confirmed by assessing the location of empirical

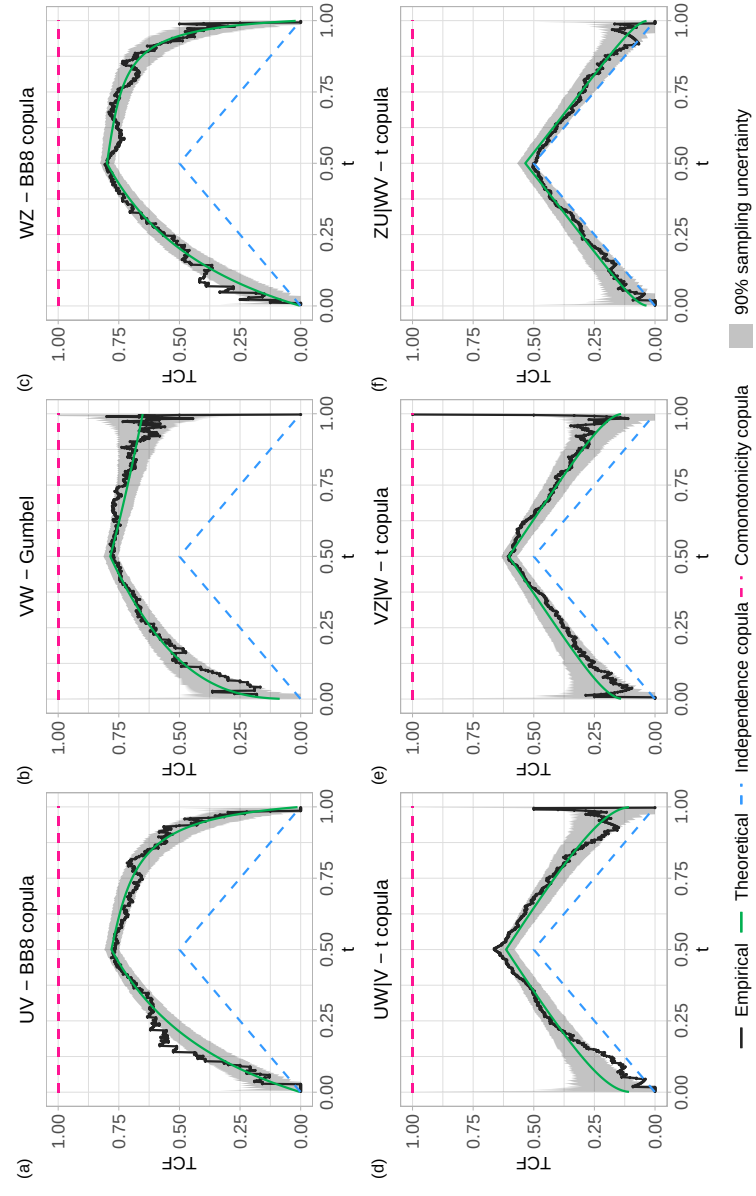

Figure 4.19: Empirical (black line with dots) and theoretical (green line) TCF of each (conditional) bivariate copula of the obtained D-vine copula along with the related 90% sampling uncertainty interval. The theoretical TCF of the independence (dashed blue line) and comonotonicity (dashed magenta line) copulas are also reported in each graph. The (conditional) copula to which each graph refers is indicated in the title by reporting the related subscript.

	$NRMSE$		NAD
	Kendall function λ-function	TCF	Kendall's tau
C_{UV}	0.096	0.082	0.006
C_{VW}	0.08	0.094	0.009
C_{WZ}	0.091	0.076	0.012
$C_{UW\|V}$	0.06	0.156	0.041
$C_{VZ\|W}$	0.07	0.138	0.018
$C_{UZ\|VW}$	0.032	0.086	0.11

Table 4.7: Performance measures values used to quantify the adequacy of the (conditional) bivariate copulas of the obtained D-vine. The $RMSE$ related to the Kendall function and λ- function and TCF and the NAD related to Kendall's tau are reported for each (conditional) bivariate copula.

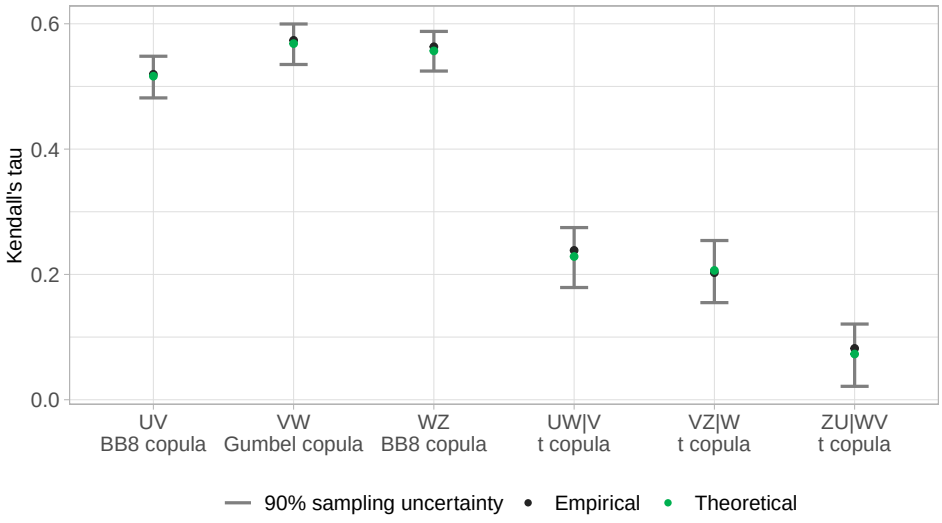

Figure 4.20: Empirical (black dots) and theoretical (green dots) of each (conditional) bivariate copula of the obtained D-vine copula along with the related 90% sampling uncertainty interval.

estimates of the considered quantities with respect to the related 90% sampling uncertainty interval of the copula. For most pair-copulas, more than 90% of the empirical estimates of all considered quantities fall within the relevant uncertainty interval. The copulas and quantities for which this percentage is less than 90% are the following:

- the BB8 copula of the variables pair (U, V) in terms of Kendall function and λ-function. For this copula and quantity, the 84% of the empirical estimates is within the related uncertainty intervals;
- the t copula of the conditional variables pair $(F_{U|V}, F_{W|V})$ in terms of TCF. The TCF sampling uncertainty interval of this copula comprises 88% of the empirical estimates.

It is worth noting that most of the empirical estimates outside of the related uncertainty intervals correspond to t values lower than 0.75 in both cases, namely for values of t not of interest for the following scenarios estimate. Therefore, overall it can be considered acceptable that the (conditional) pseudo-observations derive from the relative (conditional) bivariate copulas.

As regards the overall D-vine results, a random sample of size 1000 generated from the obtained D-vine copula is shown in Figure 4.21 along with the pseudo-observations of the investigated variables. For all variables pairs, it is possible to notice a satisfactory overlapping between the pseudo-observations and the simulated sample.

Moreover, Figure 4.22 shows the theoretical (estimated by simulation) and empirical Kendall function and λ-function of the four-dimensional D-vine along with the related 90% sampling uncertainty intervals and theoretical functions of the independence and comonotonicity copula. As evident, the D-vine copula reproduces satisfactorily the empirical Kendall function and λ-function for all values of t. Moreover, all the empirical points are within the 90% sampling uncertainty intervals and the resulting $NRMSE$ is equal to 0.012.

As regards the TCF, in Figure 4.23, the bivariate TCF between variables pairs not directly modelled by the obtained D-vine copula (i.e. (U, W), (U, Z) and (V, Z)) are shown with the related 90% sampling uncertainty intervals and theoretical functions of the independence and comonotonicity copula. For completeness, also the TCF of the other variables pairs are reported although already shown in Figure 4.19. From Figure 4.23(b), (c) and (e) it is possible to notice satisfactorily reproduction of the empirical TCF by the theoretical ones, especially considering that the dependence between these variables pairs is not directly modelled by the D-vine copula. The empirical TCF trends are captured for all variables pairs and, for

Variables pair	NAD
UV	0.016
UW	0.033
UZ	0.053
VW	0.021
VZ	0.033
WZ	0.023

Table 4.8: NAD related to Kendall's tau for all possible variables pairs.

each, more than 90% of the empirical estimates are inside the corresponding sampling uncertainty interval. The resulting $NRMSE$ related to (U, W), (U, Z) and (V, Z) are equal to 0.072, 0.093 and 0.084, respectively: values satisfactory and consistent with the TCF $NRMSE$ of the directly modeled variables pairs (Table 4.7).

Satisfactorily results related to the overall D-vine are obtained also in terms of Kendall's tau, as shown in Figure 4.24. The theoretical Kendall's tau values (obtained by simulation) are very close to the empirical ones, which are always within the related 90% sampling uncertainty intervals. In addition, the NAD for each variables pair is reported in Table 4.8. From this table it is possible to notice that the empirical Kendall's tau better reproduced are the ones related to variables pairs directly modelled by the D-vine copula, namely (U, V), (V, W) and (W, Z) (Figure 4.16). Instead, the worst reproduced dependence is that between the variables U and Z, namely between the variables pair whose dependence structure is regarded only in the t copula of the last tree. Overall, however, all the obtained NAD can be deemed satisfactorily.

As a result, the copula-related quantities used to validate the D-vine copula show that the obtained four-dimensional copula is adequate for reproducing the dependence structure between the investigated variables, mainly for high non-exceedance probabilities levels. In addition, considering the upper tail dependence results, it is possible to notice the flexibility of the D-vine in reproducing the different characteristics of the dependence structure between the investigated variables pairs. Both the strong upper tail dependence between (V, W) and the weak one between the other variables pairs are reproduced by the obtained D-vine. Hence, the resulting D-vine copula can be used to estimate the desired scenarios.

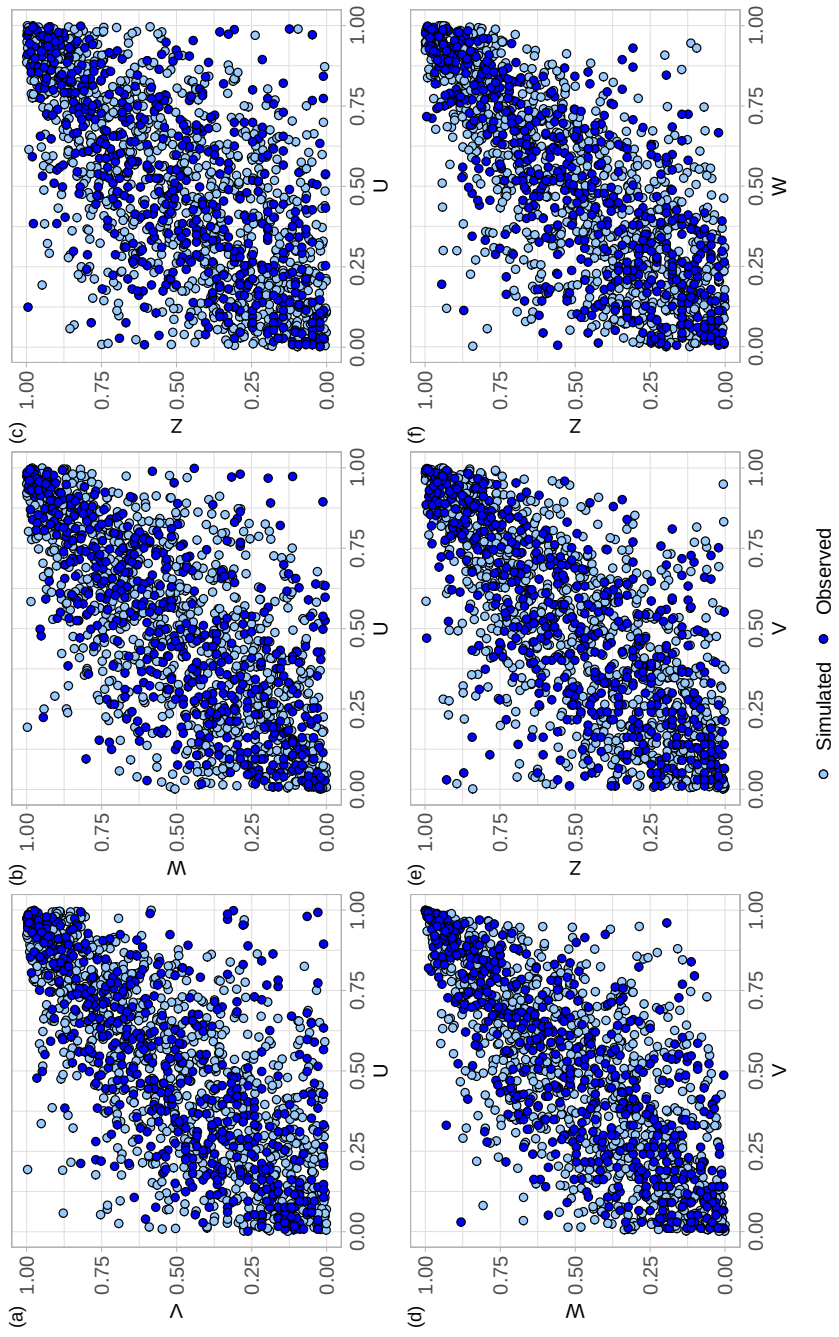

Figure 4.21: 1000 size random sample generated from the obtained D-copula and the pseudo-observations of the investigated variables.

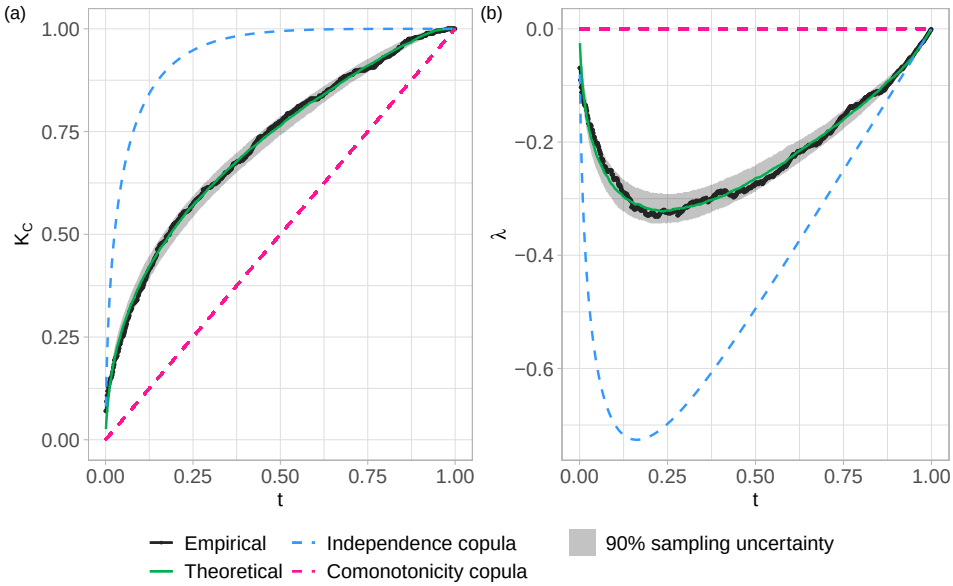

Figure 4.22: Empirical (black line with dots) and theoretical (green line) (a) Kendall function and (b) λ-function of the four-dimensional D-vine copula along with the related 90% sampling uncertainty interval. The theoretical functions of the independence (dashed blue line) and comonotonicity (dashed magenta line) copulas are also reported in both graphs.

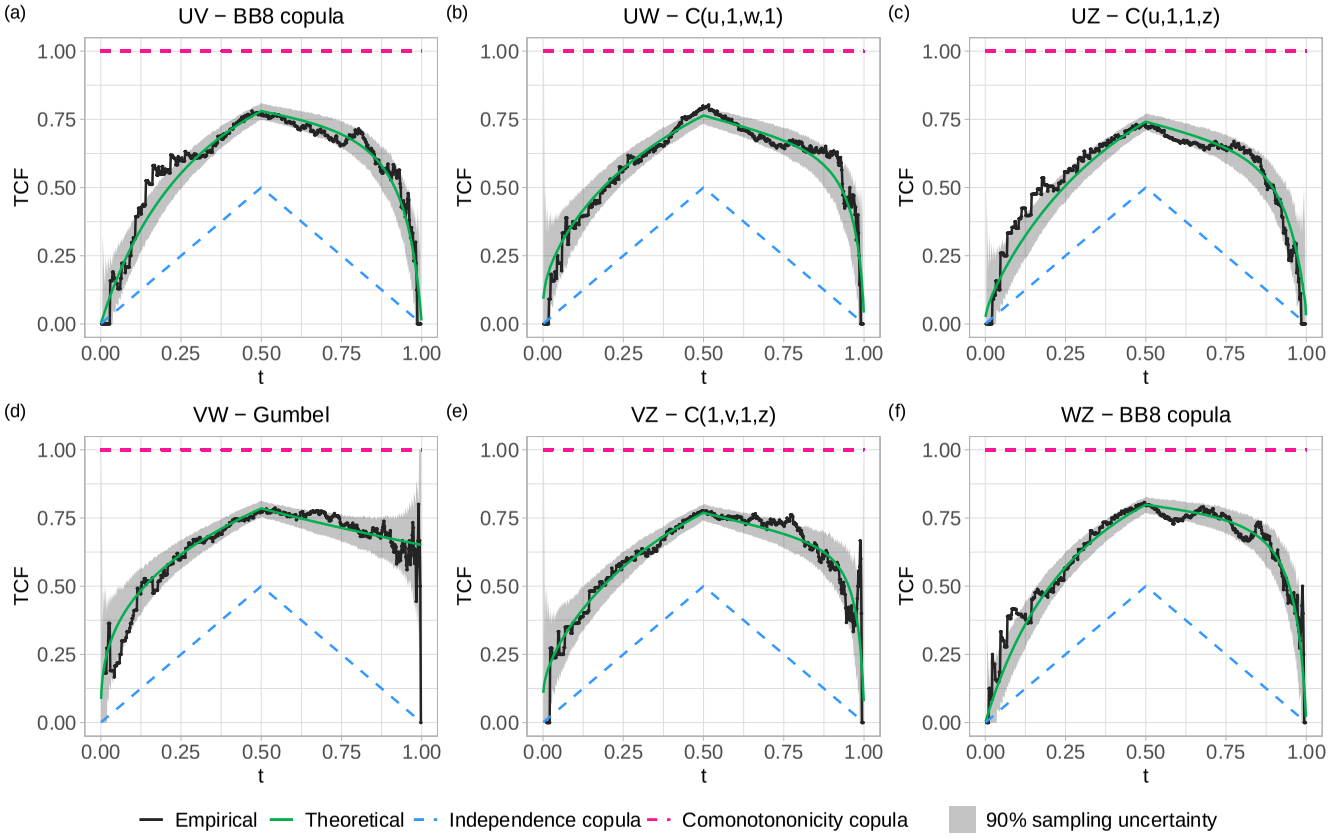

Figure 4.23: Empirical (black line with dots) and theoretical (green line) TCF of each possible investigated variables pairs obtained from the four-dimensional D-vine copula along with the related 90% sampling uncertainty interval. The theoretical TCF of the independence (dashed blue line) and comonotonicity (dashed magenta line) copulas are also reported in each graph. The copula to which each graph refers is indicated in the title and C indicates the obtained D-vine copula. The plots (a), (d) and (f) are exactly the same of Figure 4.19(a), (b) and (c), respectively.

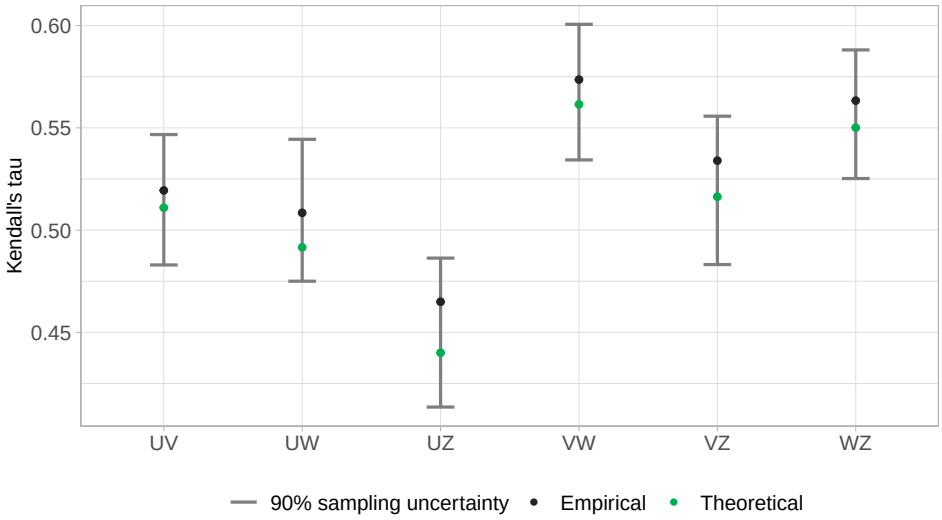

Figure 4.24: Empirical (black dots) and theoretical (green dots) of each pseudo-observations pairs along with the related 90% sampling uncertainty interval.

	t_{OR}	t_{AND}	t_K
30 years	0.9989	0.9989	0.9698
100 years	/	/	0.9809
200 years	/	/	0.9851

Table 4.9: Level t related to each considered definition and value of return period T.

4.5.4 Isohypersurfaces and scenarios

As described in Section 4.4.4, the scenarios considered in this analysis are the ones related to $T_{OR} = T_{AND} = 30$ years and $T_K = 30, 100, 200$ years. The level t related to each definition and value of the return period are reported in Table 4.9. Considering $T_{OR} = T_{AND} = T_K = 30$ years, the t levels related to the OR and AND case are exactly the same while t_K, according to Figure 4.22(a) and by definition, is lower.

For each level t of Table 4.9, the related resulting isohypersurface is shown as two-dimensional projections on the unit planes of all possible variables pairs to appreciate its shape. The critical layer of the D-vine copula of level $t = t_{OR} = 0.9989$ is shown in Figure 4.25 while the survival critical layer of the survival function of the D-vine copula of level $1 - t = 1 - t_{AND} = 1 - 0.9989$ is depicted in Figure 4.26. Moreover, the critical layers of the D-vine copula of levels $t = t_K = 0.9698, 0.9809, 0.9851$

are shown in Figure 4.27.

As evident from Figure 4.25, the identified four-dimensional points that belong to the desired isohypersurface are characterized by variables values that are always higher than the considered t_{OR} value, to which they tend asymptotically. Hence, all variables assume values in the interval $(0.9989, 1)$. In addition, all the projections of the isohypersurface, but the one related to the variables pair (V, W), are characterized by a substantial linear lower bound. Instead, the projection of the isohypersurface on the unit plane (V, W) presents a curved lower bound and thus includes lower values couples than the other variables pairs. It is worth noting that, for each variable, the mean distance between two successive isohypersurface points, ordered in ascending order based on the variable considered, is about $3 \cdot 10^{-7}$ which is considered sufficient for isohypersurface satisfactory identification.

As regards the survival critical layer of level $1 - t_{AND}$, the variable values of the detected four-dimensional points that belong to the desired isohypersurface are always lower than the considered t_{AND} value, which they asymptotically tend. As a result, all variables have values in the range $(0, 0.9989)$. Coherently with the previously described case, the shapes of the two-dimensional projections of the isohypersurface are very similar for all pairs of variables except for the variables pair (V, W) which slightly extends more in the upper right corner and thus includes higher couples of values than the other variables pairs. However, it is important to underline that the number of the four-dimensional points used to define this isohypersurface is considered not sufficient to adequately represent it. Indeed, for each variable, the mean distance between two successive isohypersurface points, ordered in ascending order based on the variable considered, is about $3 \cdot 10^{-4}$. The number of points used to define this isohypersurface is low due to the very high computational times needed to solve Eq. (4.71): about 40 days for 5000 points, using 60 cores of 3 CPU Intel® Xeon® Gold 6252N (Base Frequency: 2.30 GHz; Max Turbo frequency 3.60 GHZ). Moreover, it is worth noting that this isohypersurface includes points with low variables values, i.e. low non-exceedance probabilities. However, as evident from Figure 4.13, the marginal distributions, involved in the MLDR selection, are not able to correctly represent the behaviour of the observations for such low probabilities values. Hence, both the computational times and method of estimating marginal distributions make the definition of the AND scenario problematic and, for this reason, this scenario is not further investigated in this analysis.

The last identified isohypersurfaces are the ones related to the Kendall case. Coherently with the isohypersurface related to the OR case, the

four-dimensional points that define each isohypersurface are characterized by variables values that are always higher than the related t_K value, to which they tend asymptotically. As regards the isohypersurfaces projections shapes, the variables pairs (U, V) and (U, Z) are characterized by projections with substantial linear lower bounds while it is possible to notice curved lower bounds for the projections related to the other variables pairs. According to the previously described cases, the lower bounds of the isohypersurfaces projections on the plane (V, W) exhibit the highest curvatures and thus includes lower values couples than the other variables pairs. Similarly to the OR case, the number of points used to define each isohypersurfaces related to the Kendall case is deemed sufficient for their satisfactory identification. Indeed, for each variable, the mean distances between two successive isohypersurfaces points, ordered in ascending order based on the variable considered, related to $t_K = 0.9698, 0.9809, 0.9851$ are about $6 \cdot 10^{-6}$, $4 \cdot 10^{-6}$ and $3 \cdot 10^{-6}$, respectively.

In order to assess the effects of the dependence structure between variables on the return period estimate and variable values, for each point belonging to the satisfactorily defined isohypersurfaces, the corresponding return periods assuming an independence and perfect positive dependence condition between variables are considered. As regards the points belonging to the critical layer of level t_{OR}, the related values of the independence and comonotonicity copula and consequent T_{OR} are computed for each point and the result is shown in Figure 4.28. As evident from Figure 4.28(a), the assumption of a perfect dependence condition between variables leads to T_{OR} that are always greater than the one related to the D-vine value (orange dashed line) while the opposite occurs considering an independence condition. Furthermore, T_{OR} calculated using the independence copula values are on average closer to the D-vine T_{OR} than the ones computed using the comonotonicity copula: the mean T_{OR} assuming an independence and perfect positive dependence condition are equal to about 26 and 54 years, respectively. This highlights that, at level $t_{OR} = 0.9989$, the dependence structure between variables modelled by the D-vine copula is close to the independent one. Moreover, according to Figure 4.25, the box plots of the values of the variables on the critical layer of level t_{OR} (Figure 4.28(b)) show that V and W are the variables that on average assume the lowest values along the isohypersurface. This is due to the dependence between V and W that, for such high value of t_{OR}, is the most (and assumable as the only) significant one (Figure 4.23). As a result, the dependence between V and W is the one that has the greatest influence on obtaining D-vine copula values higher (albeit slightly) than the independence copula ones.

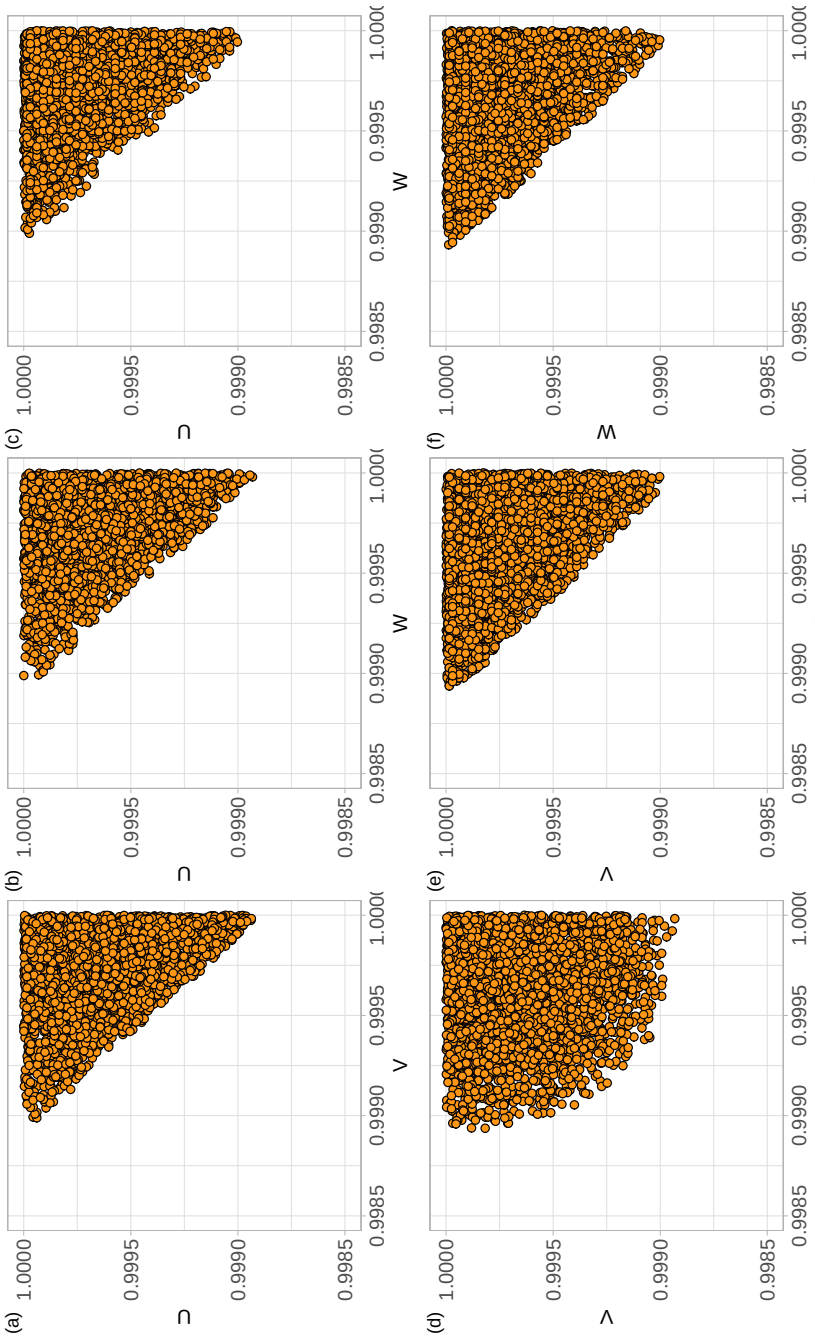

Figure 4.25: Scatterplot for each variables pair of the isohypersurface $\mathcal{L}_t$ with $t_{OR} = 0.9989$ related to $T_{OR} = 30$ years.

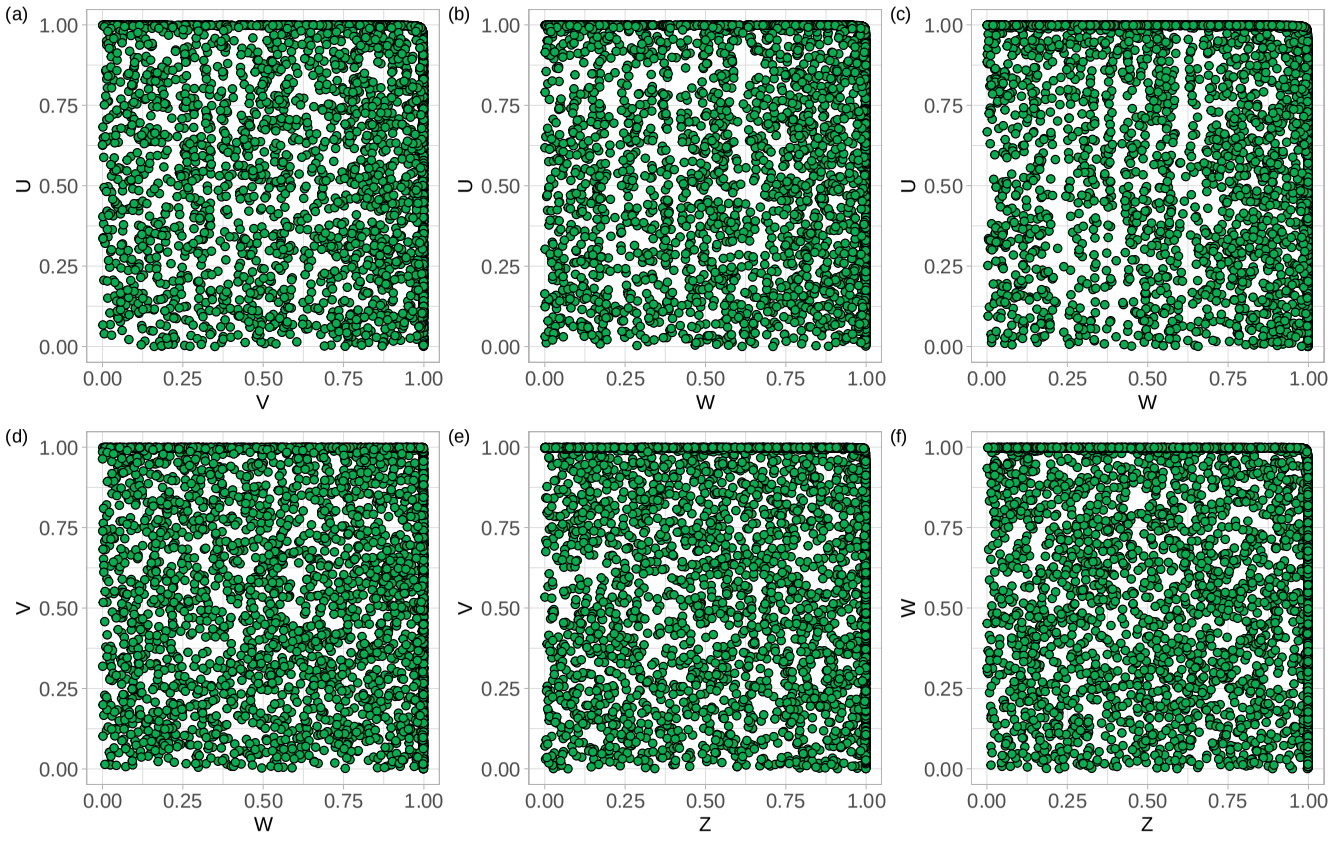

Figure 4.26: Scatterplot for each variables pair of the isohypersurface $\overline{\mathcal{L}}_{1-t}$ with $1 - t_{AND} = 1 - 0.9989$ related to $T_{AND} = 30$ years.

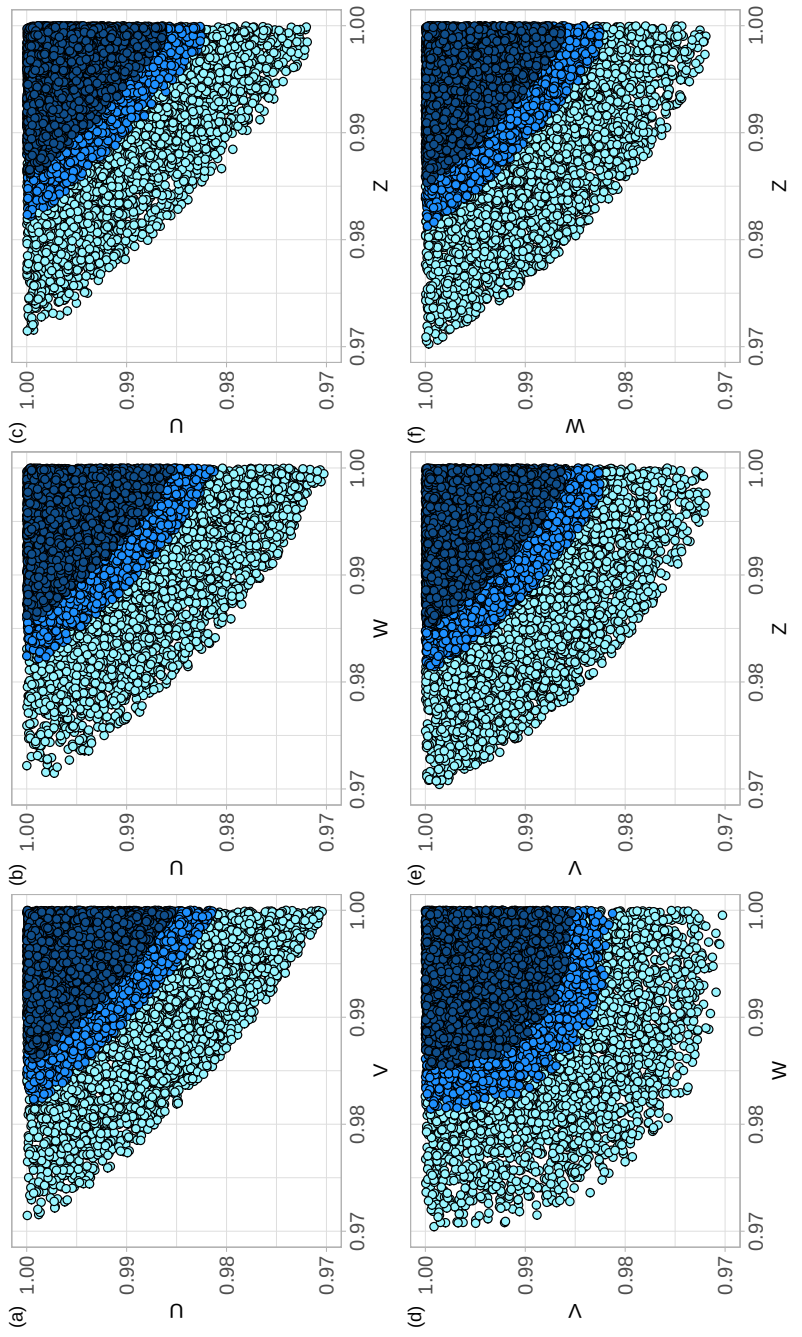

Figure 4.27: Scatterplot for each variables pair of the isohypersurfaces $\mathcal{L}_t$ with $t_K = 0.9698$ (cyan dots), $t_K = 0.9809$ (sky blue dots) and $t_K = 0.9851$ (dark blue dots) related to $T_K = 30, 100, 200$ years, respectively.

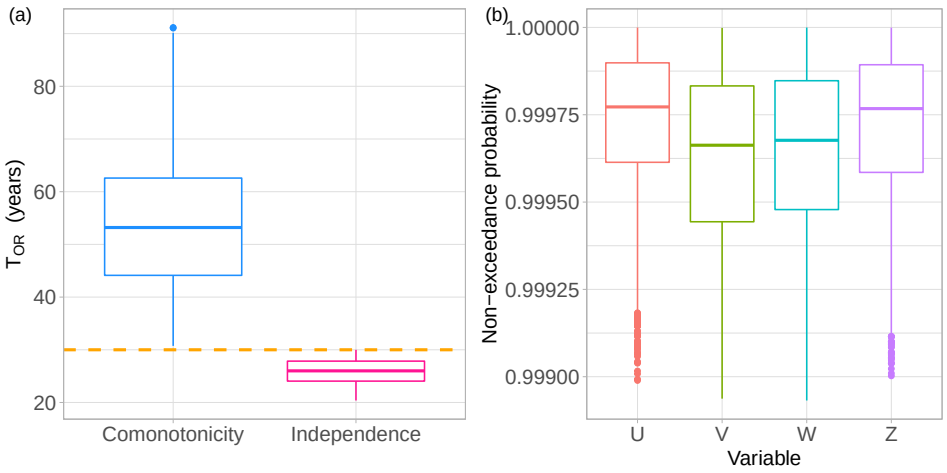

Figure 4.28: (a) Box plots of T_{OR} of the points belonging to the isohypersurface of level $t_{OR} = 0.9989$ assuming a perfect dependence and an independence condition between variables. The orange dashed line represents $T_{OR} = 30$ years namely the return period of the points according to the D-vine copula value. (b) Box plots of the values assume by variables on the isohypersurface of level t_{OR}.

As for the Kendall case, for all points of each considered isohypersurfaces, the corresponding independence and comonotonicity copula values are computed and the return period T_K are estimated introducing the related theoretical Kendall functions (Figure 4.22(a)). The results for the considered t_K are shown in Figure 4.29, 4.30 and 4.31. As evident, for all levels t_K, T_K computed assuming the independence condition between variables are much greater than the D-vine related ones. Indeed, for all critical layers, while the independence copula values at the isohypersurface's points are always lower than the corresponding D-vine copula value, the associated values of the independence Kendall function are always significantly greater than the related D-vine Kendall function one. Instead, assuming perfect positive dependence between variables results in T_K that are lower than those associated with the D-vine. Indeed, for all critical layers, the probability that the comonotonicity copula is larger than the same copula values at the isohypersurface's points is always lower than the related D-vine Kendall function value. In terms of values of the variables on the critical layers, in line with the OR case, V and W are the variables with the lowest average values for all isohypersurfaces (Figure 4.29(b), 4.30(b) and 4.31(b)). This results from the fact that the dependence between V and W is the strongest one also at the considered levels t_K of the D-vine copula (Figure 4.23). However, it is worth noting that also the dependencies be-

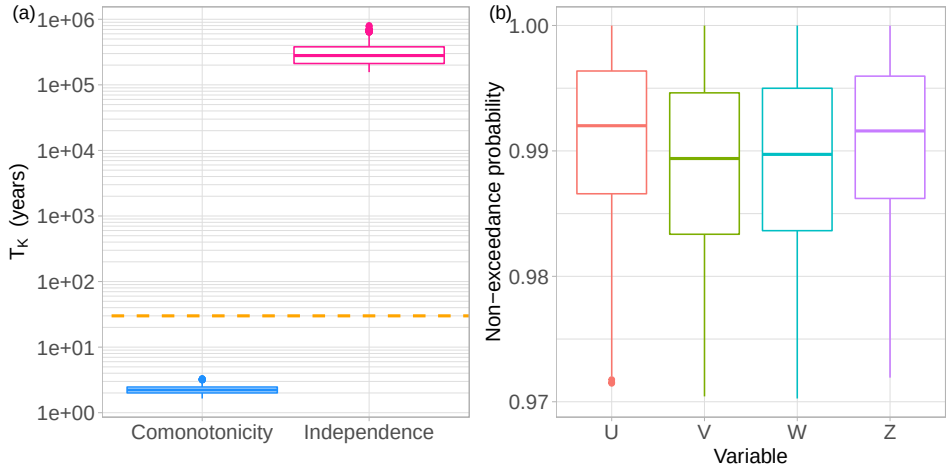

Figure 4.29: (a) Box plots of T_K of the points belonging to the isohypersurface of level $t_K = 0.9698$ assuming a perfect dependence and an independence condition between variables. The orange dashed line represents $T_K = 30$ years namely the return period of the points according to the D-vine copula value. (b) Box plots of the values assume by variables on the isohypersurface of level $t_K = 0.9698$.

tween the other possible variables pairs are not negligible at the considered levels t_K and contribute to obtaining a dependence structure that differs significantly from the independent one.

Finally, for each considered definition and value of T, the scenario is defined by selecting the MLDR and transforming back the selected copula points to the real scale. For all scenarios, the non-exceedance probabilities, marginal distributions quantiles and 90% confidence interval related to both MLDR selection and marginal CDF quantile estimate are reported in Table 4.10. Moreover, Figure 4.32 shows all the scenarios' points alongside the observations, to compare their positions in the two-dimensional planes, as well as an observations-size sample simulated from the obtained multivariate model, to visually further confirm the goodness of fit of the D-vine copula at the real scale.

As evident, the OR scenario's quantiles are the highest and exceed the values of the observations. The related non-exceedance probabilities assume very close values and, for this reason, the two-dimensional projections of the scenario's points are almost located over the related equal quantiles lines for each pair of variables. In addition, the 90% confidence interval related to the marginal CDF quantiles estimate has a relative width with respect to the related quantile that ranges between 23% and 31%. As for the 90% confidence interval of the MLDR selection, mainly the identification of the

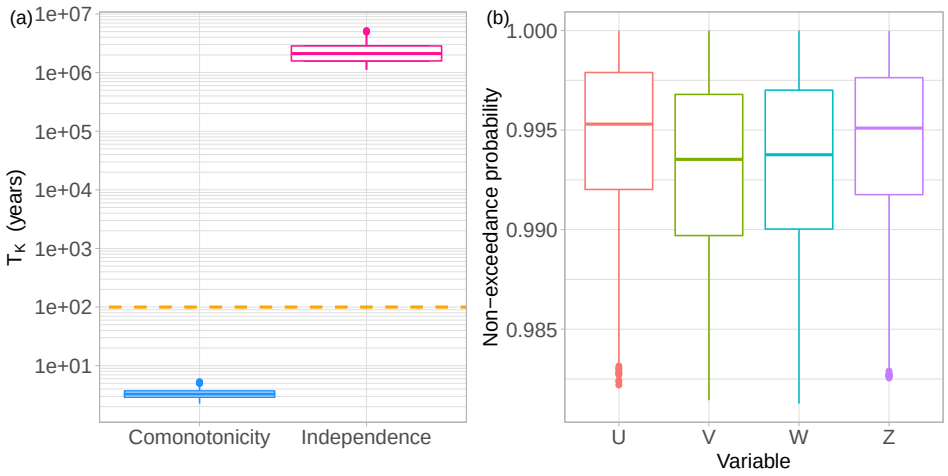

Figure 4.30: (a) Box plots of T_K of the points belonging to the isohypersurface of level $t_K = 0.9809$ assuming a perfect dependence and an independence condition between variables. The orange dashed line represents $T_K = 100$ years namely the return period of the points according to the D-vine copula value. (b) Box plots of the values assume by variables on the isohypersurface of level $t_K = 0.9809$.

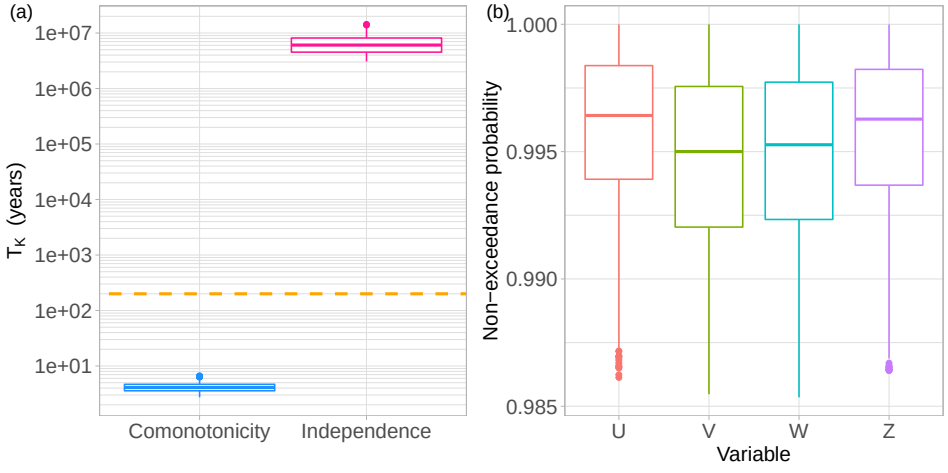

Figure 4.31: (a) Box plots of T_K of the points belonging to the isohypersurface of level $t_K = 0.9851$ assuming a perfect dependence and an independence condition between variables. The orange dashed line represents $T_K = 200$ years namely the return period of the points according to the D-vine copula value. (b) Box plots of the values assume by variables on the isohypersurface of level $t_K = 0.9851$.

	OR scenario	Kendall scenario		
	30 years	30 years	100 years	200 years
U	0.999697	0.987876	0.992344	0.994550
H_P (mm)	178	85	96	104
90% CI MLDR u (mm)	177 - 179	84 - 85	95 - 99	104 - 106
90% CI $G_P^{-1}(u)$ (mm)	150 - 205	75 - 96	84 - 108	91 - 118
V	0.999666	0.990288	0.993867	0.995556
H_M (mm)	128	70	77	83
90% CI MLDR v (mm)	127 - 128	69 - 71	77- 79	81 - 83
90% CI $G_M^{-1}(v)$ (mm)	110 - 143	62 - 75	69 - 84	73 - 91
W	0.999695	0.991170	0.994424	0.995636
H_{PT} (mm)	131	76	83	87
90% CI MLDR w (mm)	130 - 131	75 - 76	83 - 83	87 - 89
90% CI $G_{PT}^{-1}(w)$ (mm)	113 - 145	69 - 81	75 - 90	78 - 94
Z	0.999596	0.987610	0.993469	0.994434
H_C (mm)	77	45	52	53
90% CI MLDR z (mm)	77 - 77	44 - 45	50 - 52	52 - 53
90% CI $G_C^{-1}(z)$ (mm)	70 - 87	42 - 49	48 - 56	49 - 58

Table 4.10: Most-likely design realizations for each considered definition and value of T: $T_{OR} = 30$ years, $T_K = 30, 100, 200$ years. For each scenario, the following quantities are reported: (i) the non-exceedance probabilities provided by the D-vine copula (i.e. values of the variables U, V, W and Z, respectively), (ii) the related quantiles of the marginal distributions (i.e. values of the variables H_P, H_M, H_{PT} and H_C), (iii) the 90% confidence interval (CI) related to the MLDR selection and (iv) the 90% confidence interval of the marginal distributions quantiles estimate at the related non-exceedance probabilities.

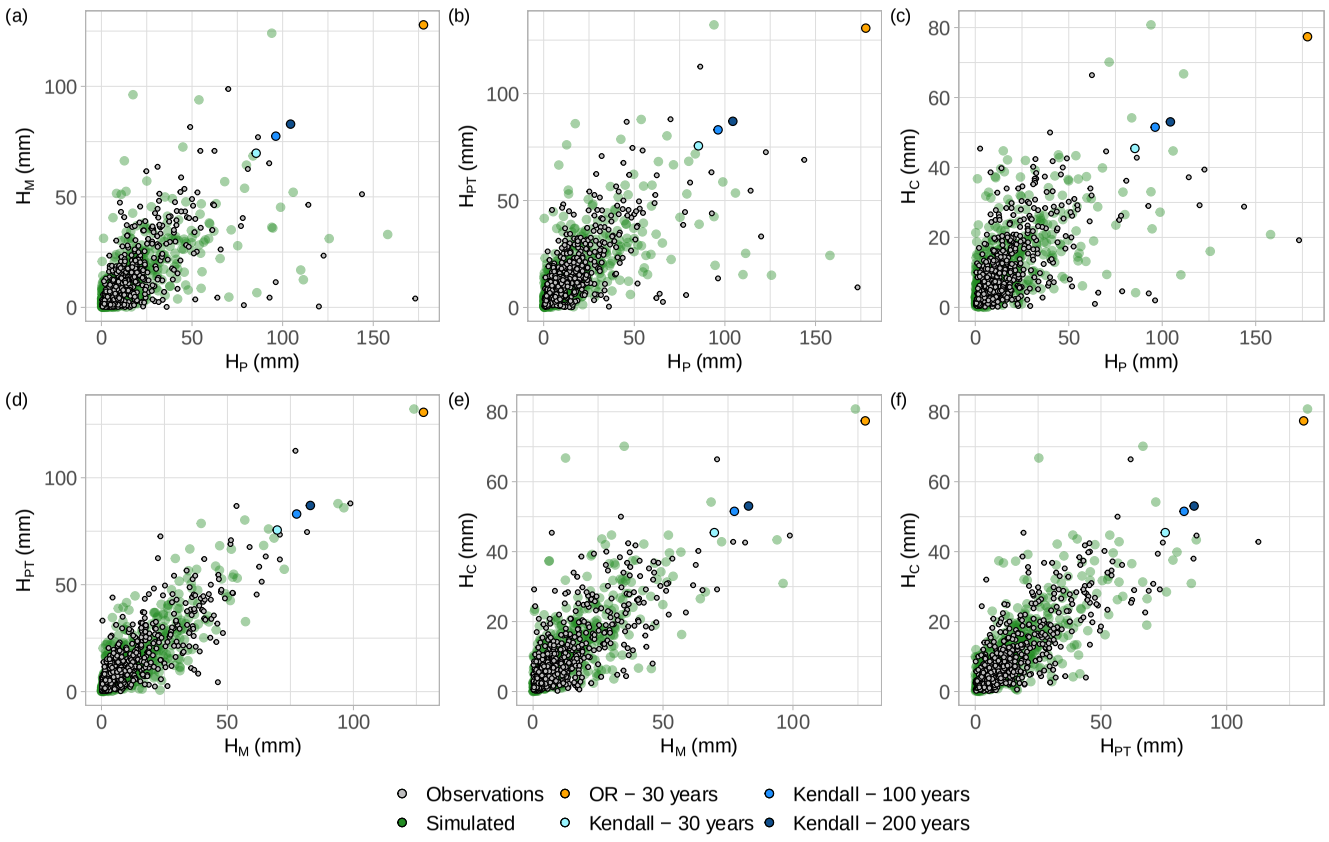

Figure 4.32: OR scenario for $T_{OR} = 30$ years and Kendall scenarios for $T_K = 30, 100, 200$ years along with the observations and a observations-size simulated sample.

isohypersurfaces of level t_{OR} with a sufficiently large number of points makes it very narrow for all variables.

As regards the Kendall scenarios, the related quantiles fall within the range of variability of the observations and the related non-exceedance probabilities assume similar values. Hence, for each combination of variables, all the two-dimensional projections of the Kendall scenarios' points are close to the related equal quantiles lines. Moreover, thanks to the lower values of the probabilities, the 90% confidence intervals related to the marginal CDF quantiles estimate have lower relative width with respect to the related quantile than the OR scenario's ones and they vary between 14% and 24% for $T_K = 30$ years, 16% and 25% for $T_K = 100$ years and 16% and 26% for $T_K = 200$ years. In addition, according to the OR scenario, the 90% confidence intervals of the MLDR selection are very narrow for all variables and scenarios.

4.5.5 Possible use of the obtained scenarios with a hazard mapping purpose

The obtained scenarios, and in particular the Kendall ones, are promising to be used to assess the effects of the related precipitation forcing on the study area with a hazard mapping purpose by:

- evaluating the possible triggering of a debris flow in the Rotiano catchment and its magnitude related to the 24h cumulative rainfall in P;
- estimating the flood wave in the Noce river at the confluence due to the 24h cumulative rainfall in M, PT and C;
- simulating these compound phenomena at the confluence.

As regards the precipitation forcing related to a given scenario, the synthetic hyetograms at each considered rain gauge can be defined, for instance, with an hourly interval assuming a constant rainfall intensity in M, P and C since no analyses are performed in this study regarding the distribution of the rainfall in the related 24h time windows. Instead, given the assumptions introduced for the definition of the synchronous event, the synthetic hyetogram in P should be characterized by the maximum hourly rainfall intensity at the end of the rainfall event. In addition, the timing of the investigated hazardous phenomena assumed to define the synchronous event, has to be considered by introducing a time shift of 3 hours between the hyetogram in P and those in M, PT and C.

Moreover, the simulation findings can also be used to assess if the precipitation forcing determines the timing of co-occurrence of the investigated

phenomena at the confluence, hypothesized for the definition of synchronous events, and if this co-occurrence is the most dangerous at the confluence.

Finally, it is worth noting that the scenarios are selected, among possible, based on a purely statistical approach that identifies the most likely ones. However, given a scenario, not necessarily the most likely combination is also the one that determines the most severe impacts at the confluence. For this reason, it can be useful to consider different combinations of hydrological forcing with selected return period, applying for instance the method proposed in Volpi and Fiori (2012), thus identifying the one with the most dangerous effects.

4.6 Final remarks

In this work, a multivariate model is developed to obtain rainfall scenarios with a multi-hazard assessment purpose of a confluence between a creek susceptible to debris flows and a flood-prone river. The analysis is based on rainfall data of four selected rain gauges: one for the catchment prone to debris flows and three for the basin potentially subject to floods. A sampling strategy is developed to identify synchronous events and compute the related observations consisting of 24h cumulative rainfall in each rain gauge, taking into account the timing between the investigated phenomena. The SMEV formulation is then applied for the univariate analysis of extreme values. Hence, the dependence structure between observations is quantified and modelled with a four-dimensional vine copula. Finally, rainfall scenarios related to different definitions and values of multivariate return period are estimated based on the thus built multivariate model.

As regards the synchronous events set, the mutual distances between the considered rain gauges, in particular between P and the other rain gauges, and their locations seem to affect both the observations values and dependence structure, mainly in terms of overall correlation. However, it would be necessary to analyze more rain gauges to obtain robust results regarding these aspects.

In terms of the multivariate model, the univariate analysis demonstrates that the two-parameter Weibull distribution is adequate for replicating the right-tail of each investigated variable's observations, corroborating what has already been proven by earlier studies. Moreover, the obtained D-vine copula reproduces satisfactorily the different characteristics of the dependence structure between the variables' observations, characterized by a high overall correlation between all variables pairs and both weak and strong upper tail dependence depending on the considered variables pair. This

confirms the ability of the pair-copula construction method in building a flexible multivariate copula.

As regards the scenarios computation, due to the high dimension of the copula and the marginal distributions fitting method, the analysis of the isohypersurface related to the AND case highlights some issues in its estimate and use. Coherently with the dependence structure, the OR isohypersurface's points and the related scenario differ in a substantially negligible way from those provided by the independence copula at the considered copula level. Instead, considering the Kendall case, the values of the probability distribution of the obtained D-vine copula at the isohypersurface's points are significantly different from the independence copula probability values at the same points. As a result, the scenarios related to the Kendall case are characterized by a much greater return period assuming a condition of independence. This means that, for the analyzed return periods, taking into account the dependence structure between variables provides 24h cumulative rainfall in each rain gauge that are higher than those obtainable by adopting a condition of independence.

The employ of the SMEV formulation for the analysis of extreme values allows the construction of a multivariate model based on all available observations of the process under investigation, regardless of their values. Hence, the method proposed in this work is different from the classical literature approaches applied to assess compound extreme events, which usually rely on annual maxima or peak over threshold method to identify the process realizations to be used in the analysis (e.g. Brunner et al., 2016, Camus et al., 2021, Ghizzoni et al., 2010, Mujumdar et al., 2018, Sadegh et al., 2018). As a result, the SMEV approach made it possible to exploit all information provided by the realizations of the investigated process, in terms of both univariate marginal and dependence structure between variables analysis. Further studies are needed to assess the differences between the multivariate model obtained using the SMEV approach and the ones deriving from the classical literature approaches. In terms of dependence structure, this comparison results in evaluating how much the use of all the observations determines a multivariate copula different from the one resulting from considering only observations, for instance, above arbitrary thresholds at the same time in each rain gauge. It is worth noting that, in a multivariate framework, the annual maxima approach cannot be directly applied unless the annual maxima occur simultaneously in all the rain gauges considered. Otherwise, a multivariate analysis of annual maxima just informs on the joint probability of occurrence in the same year without taking into account their timing within that year (Blanchet et al., 2018, Brunner et al., 2019).

The comparison between the SMEV-based and classical EVT-based dependence structure models has to be performed by computing the levels of each investigated copula that determine the same arbitrary return period and estimating the related isohypersurfaces and scenarios.

In conclusion, this work has set the stage to construct actual multi-hazard maps based on rainfall scenarios estimated taking into account the correlation between the investigated phenomena' main drivers, namely the rainfall at reference rain gauges. Using these scenarios it is possible to assess the effects, at the considered confluence, resulting from the investigated compound phenomena with a given multivariate return period, introducing proper hydrology and hydraulic modelling. The simulation results can also be used to optimize the multivariate model, in terms of synchronous events definition and scenario selection. Moreover, the methodological scheme developed in this study can also be applied to other types of compound events characterized by drivers that can result in simultaneous hazardous phenomena.

Part III

Public awareness within the LIFE FRANCA project

Chapter 5

The LIFE FRANCA European project

5.1 General framework and project overview

Public awareness and preparedness, as well as the development of a complete understanding of hydrogeological phenomena mitigation, are crucial components of hydrogeological risk mitigation (UNISDR, 2004). In both peacetime and emergency situations, a well-informed and prepared population can take preventative measures to decrease their vulnerability and exposure to hazards.

Because of the shift in risk mitigation paradigm from hazard elimination to vulnerability and exposure reduction, the population's active engagement in risk management is becoming increasingly important. In this framework, residents of flood-prone areas are considered responsible actors in risk management (Maidl and Buchecker, 2015), and they share responsibility for the consequences of a flood event with public authorities (Papagiannaki et al., 2019b), according to an integrated flood risk management promoted, among other things, by the European Flood Directive (2007/60/CE) (e.g. Martinengo et al., 2021a).

The LIFE FRANCA (Flood Risk ANticipation and Communication in the Alps) European project fitted into this context, with the goals of: (i) promoting a flood risk prevention culture, (ii) introducing an anticipatory method in the flood risks management, (iii) developing a proper communication strategy, (iv) preparing the public to deal with floods by involving residents, experts, and decision-makers in a participatory approach. The project's reference area was the Alps, namely the Autonomous Province of Trento (Italy), with citizens, students, teachers, technicians, administrators,

and journalists as stakeholders. The project partners were:

- the University of Trento, Department of Sociology and Social Research and Department of Civil, Environmental and Mechanical Engineering;
- the University of Padova, Department of Land, Environment, Agriculture and Forestry;
- the Autonomous Province of Trento, Service for Torrent Control;
- the Eastern Alps District Authority;
- MUSE - Science Museum, Trento;
- Trilogis Srl.

Throughout the project, the partners collaborated on numerous fronts and communication methods, involving all stakeholders to establish a flood risk culture and better categories functioning in the field of flood risk. The project has been characterized by eight (interconnected) actions:

- Reorganisation and data analysis: review of the literature and existing approaches for visual communication of flood risk; gathering and analysis of available data on the Autonomous Province of Trento flood hazard. The information gathered was used to develop the flood risk portal as well as strategic scenarios for the project study areas;
- Analysis of flood risk perception: investigation of flood risk knowledge and perception of citizens and stakeholders involved in flood risk management and communication, using web surveys, paper questionnaires, and interviews;
- Construction of strategic scenarios and focus groups: elaboration, in collaboration with stakeholders and municipalities, of future strategic scenarios and their implications for their territory. Focus groups with residents are being organized to involve them in social anticipating exercises and to examine future scenarios;
- Building of a flood risk portal: development of an online flood risk portal that will serve as a resource for anyone (specialists, public, decision-makers) seeking up-to-date information on the hydrogeological situation in the Autonomous Province of Trento. Different people can also participate in the surveillance of the territory by using this technology;

- Communication: definition of the communication and promotion plan of the project and presentation of LIFE FRANCA to citizens and the media through various means of communication;

- Education and dissemination: planning and implementation of educational and informational initiatives directed at both students and citizens in order to promote the culture of hydrogeological risk prevention;

- Training and education: organization of courses and seminars to increase understanding of the hydrogeological risk in the Alps and enhance abilities in coping with, evaluating, and communicating flood risk to communities;

- Networking: organization of conferences, consultations, and working groups in order to disseminate the LIFE FRANCA project's results, but more importantly, to exchange information and form collaborations with other stakeholders who deal with natural risk management and communication in various capacities.

More information can be found at the LIFE FRANCA website[1], in the project layman's report[2] and final report[3] .

5.2 LIFE FRANCA and public awareness

The public awareness-raising was pursued throughout the entire project employing several strategies and addressing different stakeholders. The process of creating strategic scenarios, involving technicians, citizens and decision-makers, is an example of a strategy employed in the project. The strategic scenarios approach (Schwartz and Baer, 1991, Van der Heijden, 2005, e.g.) uses a matrix with two axes of uncertainty that, when combined, results in four possible scenarios. The uncertainty refers to factors that, within the LIFE FRANCA framework, are related to the change in the local community's approach to managing flood risks. Thanks to the selection of the most relevant and uncertain factors, the four scenarios set are expected to encompass the widest range of possibilities and offer insights into the most

[1] www.lifefranca.eu

[2] Available at:
www.lifefranca.eu/wp-content/uploads/2020/01/1219-Laymans_LifeFranca_EN-Web.pdf

[3] Available at:
www.lifefranca.eu/wp-content/uploads/2020/06/FRANCA-final-report-WEB.pdf

important uncertainties and discontinuities concerning the current situation. The strategic scenarios have been built for three case studies by three working groups in the Autonomous Province of Trento (Italy). The case studies have been selected to represent the range of socio-economic features and hydrogeological hazards present in the municipalities in the Alps. The most mentioned factors by the three groups were: changing population, communication, civic attitudes towards the common good, climate and spatial planning and land use. Once a couple of variables to be considered along the axes and their extremes have been identified, each scenario consists of a narrative and qualitative account of a particular arrangement of conceivable states for the chosen variables. The scenarios and associated narratives helped each group have thoughtful discussions. The groups have determined the most likely outcomes, the critical concerns that must be addressed going forward, as well as potential changes that, if consciously welcomed, could present opportunities. Moreover, the same scenario-building method encourages participants to have a deeper awareness of uncertainties and the procedures involved in risk management and communication.

Another example of an awareness strategy was the creation of a flood risk portal[4]. The aim is to make the portal become the primary method of communicating flood risks in the Province of Trento and serve as a hub for those who want to access and exchange knowledge about managing flood risk. The portal's primary innovation is two-way communication aimed at citizens, technicians, and decision-makers. The creation of scenarios for understanding the evolution of the territory is made easier for technicians and decision-makers with access to verified information while citizens can learn more about flooding and disaster preparedness. The possibility of making the community aware and resilient to actively participate in flood risk prevention efforts is based on the latter factor. In addition, the portal has a WebGIS in which maps related to flood risk can intuitively visualized and citizens can actively contribute to the defence of the territory by reporting any damage to the defence works or through the testimony of flood events. This direct involvement in the management of the territory aims to increase the awareness of the population and promote active participation in prevention activities.

Finally, several education and communication activities based on different informational initiatives and tools have been carried out. These activities included conferences, seminars, educational visits, educational travelling exhibitions, and courses, all conceived based on the target audience. All education and communication activities have been aimed at promoting the

[4] https://bacinimontani.provincia.tn.it

knowledge and prevention of flood risk to make the community more aware.

5.3 Training and education action

5.3.1 Method

Among other project actions, I have collaborated on the "Training and education" action. This action has been coordinated by the University of Trento - DICAM/CUDAM unit (Department of Civil, Environmental and Mechanical Engineering – University Centre for Advanced Studies on Hydrogeological Risk in Mountain Areas) which aimed to provide basic training on several hydrogeological hazard aspects (i.e. phenomenological, managerial, communicative, social and legal) as well as to analyze some risk communication features. To achieve these objectives, the main activities of this action have been the organization, management and deliverance of training sessions addressed to three groups of stakeholders: professional technicians, journalists, and policymakers.

In general, all of the courses have been designed to present a multidisciplinary perspective on hydrogeological risk, with speakers from various professional sectors (technicians, journalist, mayor, judge, jurist, risk communicator, sociologist). In particular, the main analysed topics have been:

- the hydrogeological phenomena;
- the hydrogeological risk mitigation in peacetime (e.g. hazard mapping and planning);
- the emergency situations management (emergency planning and mayors' experiences);
- the social perception of flood risk;
- the legal aspects connected to the hydrogeological risk mitigation and management (a judge point of view and the environmental laws);
- the communication of the natural hazards and the LIFE FRANCA portal;
- the strategic scenarios, developed in an other project action.

Moreover, the courses have been characterized by a field trip to some protection structures and areas affected by hydrogeological phenomena, organized in collaboration with the Autonomous Province of Trento - Service for Torrent Control.

Some images of the courses are shown in Figure 5.1.

Figure 5.1: Some photos of the courses and field trips held within the LIFE FRANCA project

5.3.2 Main results

The courses have provided comprehensive and specific training on hydrogeological risk analysing it from technical, managerial, emergency, legal, communicative and social points of view. The presence of speakers representing a variety of standpoints has allowed us to analyse the topic from various points of view. These multi-disciplinary views have resulted in proficient interactions between stakeholders and speakers that have focused mainly on peacetime and emergency phase issues. The emergency experiences reported by mayors have highlighted the difficulties related to flood risk management, especially for small municipalities. Usually, policymakers are unaware of their responsibilities related to emergency management (in Italy, the mayor is the Civil Protection authority in his/her municipality), and they are not prepared to deal with extreme events. These issues have emerged and have been discussed in all courses.

The field trips have been fundamental to contextualise the provided technical information, describing the causes and the effects of the occurred hydrogeological events and analysing the protection structures present on the territory.

In terms of participants, the courses have involved primarily munici-

pal administrators and technical professionals. Journalists have shown low interest to the courses and we have not been able to involve them.

5.4 Final considerations on the project

The major purpose of LIFE FRANCA project was to communicate and anticipate various hazards that are identified as having the greatest impact and being the most likely in the next ten years on a global scale in the Global Risk Report 2019 drawing by the World Economic Forum (WEF, 2019), namely extreme weather events and natural disasters.

The project has raised flood risk awareness in the Alpine regions, which are particularly vulnerable to extreme weather events, by implementing a customized communication and involvement approach tailored to the requirements and responsibilities of the various stakeholders in the research areas. In addition, LIFE FRANCA has launched a comprehensive initiative to prepare the public to live with natural disasters, particularly floods, through a participatory approach including residents, experts, and decision-makers, to foster a widespread feeling of public and private co-responsibility. Lastly, the project allowed dialogue for a common goal between different stakeholder groups and this resulted in proficient interactions and sharing of different points of view.

Final considerations

The challenge posed by Giuseppe Zamberletti, the founder of the Civil Protection, has been the thread of my doctoral research: "The challenge of the Civil Protection is only one: it must dream, hope and work so that, in perspective, the organization of the rescue is less and less important, in the sense that we are called to develop more and more the prevention policy and the prediction capability".

In light of this challenge, my research has tried to improve some non-structural mitigation strategies. In this work, an innovative physical-based method to calibrate debris-flow rainfall thresholds has been introduced, and the threshold obtained by applying it to a study area proved to be robust and reliable. This result sets the stage for the employ of the BDA approach to estimate stony debris-flow rainfall thresholds usable in operational EWS. Moreover, a multivariate rainfall analysis allowed for the estimate of rainfall scenarios while taking into account the correlation between the investigated phenomena' main driver at several reference locations. The generated scenarios, which are linked to different multivariate return periods, can be utilized to assess the effects of the investigated compound phenomena on the study area and, as a result, to construct actual multi-hazard maps. Lastly, the courses held within the LIFE FRANCA project gave participants a multidisciplinary perspective on hydrogeological risk thus trying to raise their awareness. The dialogue established among the various stakeholder groups has resulted in fruitful exchanges and sharing of different points of view.

Overall, the analyzes and activities carried out during my doctorate, also within research projects, enabled me to achieve the set objectives and to make a contribution, albeit small, to the topics covered. The hope is that the analyses completed and the results obtained have set the stage for actual advances in hydrogeological risk management.

Bibliography

K. Aas, C. Czado, A. Frigessi, and H. Bakken. Pair-copula constructions of multiple dependence. *Insurance: Mathematics and economics*, 44(2): 182–198, 2009.

H. Abdi. Coefficient of variation. *Encyclopedia of research design*, 1:169–171, 2010.

M. T. Abraham, N. Satyam, A. Rosi, B. Pradhan, and S. Segoni. The selection of rain gauges and rainfall parameters in estimating intensity-duration thresholds for landslide occurrence: Case study from wayanad (india). *Water*, 12(4), 2020. ISSN 2073-4441.

L. Aceto, A. Pasqua, and O. Petrucci. Effects of damaging hydrogeological events on people throughout 15 years in a mediterranean region. *Advances in Geosciences*, 44:67–77, 2017.

H. Akaike. Maximum likelihood identification of gaussian autoregressive moving average models. *Biometrika*, 60:255–265, 8 1973. ISSN 0006-3444. doi: 10.1093/BIOMET/60.2.255.

J. E. Angus. The probability integral transform and related results. *SIAM review*, 36(4):652–654, 1994.

C. N. Arachchige, L. A. Prendergast, and R. G. Staudte. Robust analogs to the coefficient of variation. *Journal of Applied Statistics*, pages 1–23, 2020.

A. Armanini, L. Fraccarollo, and G. Rosatti. Two-dimensional simulation of debris flows in erodible channels. *Computers & Geosciences*, 35(5): 993–1006, 2009.

N. Balakrishnan and M. Kateri. On the maximum likelihood estimation of parameters of Weibull distribution based on complete and censored data. *Statistics & Probability Letters*, 78(17):2971–2975, 2008.

N. Balakrishnan and C. D. Lai. *Continuous bivariate distributions*. Springer Science & Business Media, 2009.

M. Barendrecht, N. Sairam, L. Cumiskey, A. D. Metin, F. Holz, S. J. Priest, and H. Kreibich. Needed: A systems approach to improve flood risk mitigation through private precautionary measures. *Water Security*, 11: 100080, 2020.

L. R. Barnes, D. M. Schultz, E. C. Gruntfest, M. H. Hayden, and C. C. Benight. Corrigendum: False alarm rate or false alarm ratio? *Weather and Forecasting*, 24(5):1452–1454, 2009.

J. I. Barredo. Normalised flood losses in europe: 1970–2006. *Natural hazards and earth system sciences*, 9(1):97–104, 2009.

R. L. Baum and J. W. Godt. Early warning of rainfall-induced shallow landslides and debris flows in the usa. *Landslides*, 7(3):259–272, 2010.

T. Bedford and R. M. Cooke. Probability density decomposition for conditionally dependent random variables modeled by vines. *Annals of Mathematics and Artificial intelligence*, 32(1):245–268, 2001.

T. Bedford and R. M. Cooke. Vines–a new graphical model for dependent random variables. *The Annals of Statistics*, 30(4):1031–1068, 2002.

C. Bel, F. Liébault, O. Navratil, N. Eckert, H. Bellot, F. Fontaine, and D. Laigle. Rainfall control of debris-flow triggering in the Réal Torrent, Southern French Prealps. *Geomorphology*, 291:17–32, 2017.

R. Bendel, S. Higgins, J. Teberg, and D. Pyke. Comparison of skewness coefficient, coefficient of variation, and gini coefficient as inequality measures within populations. *Oecologia*, 78(3):394–400, 1989.

M. Bernard, M. Boreggio, M. Degetto, and C. Gregoretti. Model-based approach for design and performance evaluation of works controlling stony debris flows with an application to a case study at rovina di cancia (venetian dolomites, northeast italy). *Science of the total environment*, 688: 1373–1388, 2019.

M. Berti, M. Martina, S. Franceschini, S. Pignone, A. Simoni, and M. Pizziolo. Probabilistic rainfall thresholds for landslide occurrence using a bayesian approach. *Journal of Geophysical Research: Earth Surface*, 117 (F4), 2012.

E. Bevacqua, D. Maraun, I. H. Haff, M. Widmann, and M. Vrac. Multivariate statistical modelling of compound events via pair-copula constructions: Analysis of floods in ravenna. *Hydrology and Earth System Sciences Discussions*, pages 1–34, 1 2017. ISSN 1027-5606. doi: 10.5194/hess-2016-652.

C. Bisci, M. Fazzini, F. Dramis, R. Lunardelli, A. Trenti, and M. Gaddo. Analysis of spatial and temporal distribution of precipitation in trentino (italian eastern alps): Preliminary report. *Meteorologische Zeitschrift*, pages 183–187, 2004.

J. Blanchet, C. Aly, T. Vischel, G. Panthou, Y. Sané, and M. Diop Kane. Trend in the co-occurrence of extreme daily rainfall in west Africa since 1950. *Journal of Geophysical Research: Atmospheres*, 123(3):1536–1551, 2018.

H. Blijenberg. In-situ strength tests of coarse, cohesionless debris on scree slopes. *Engineering Geology*, 39(3-4):137–146, 1995.

J. V. Bonta. Characterizing and estimating spati al and temporal variability of times between storms. *Transactions of the ASAE*, 44(6):1593, 2001.

J. V. Bonta. Estimation of parameters characterizing frequency distributions of times between storms. *Transactions of the ASAE*, 46(2):331, 2003.

J. V. Bonta and A. Nayak. Characterizing times between storms in mountainous areas. *Transactions of the ASABE*, 51(6):2013–2028, 2008.

J. V. Bonta and A. R. Rao. Factors affecting the identification of independent storm events. *Journal of Hydrology*, 98(3-4):275–293, 1988.

F. Brardinoni, M. Church, A. Simoni, and P. Macconi. Lithologic and glacially conditioned controls on regional debris-flow sediment dynamics. *Geology*, 40(5):455–458, 2012.

E. C. Brechmann and U. Schepsmeier. Modeling dependence with c- and d-vine copulas: The r package cdvine. *Journal of Statistical Software*, 52: 1–27, 2 2013. ISSN 15487660. doi: 10.18637/jss.v052.i03.

P. Brufau, P. Garcia-Navarro, P. Ghilardi, L. Natale, and F. Savi. 1D mathematical modelling of debris flow. *Journal of hydraulic research*, 38 (6):435–446, 2000.

M. Brunetti, S. Peruccacci, M. Rossi, S. Luciani, D. Valigi, and F. Guzzetti. Rainfall thresholds for the possible occurrence of landslides in Italy. *Natural Hazards & Earth System Sciences*, 10(3), 2010.

M. T. Brunetti, M. Melillo, S. Peruccacci, L. Ciabatta, and L. Brocca. How far are we from the use of satellite rainfall products in landslide forecasting? *Remote sensing of environment*, 210:65–75, 2018.

M. I. Brunner, J. Seibert, and A.-C. Favre. Bivariate return periods and their importance for flood peak and volume estimation. *Wiley Interdisciplinary Reviews: Water*, 3(6):819–833, 2016.

M. I. Brunner, R. Furrer, and A. C. Favre. Modeling the spatial dependence of floods using the fisher copula. *Hydrology and Earth System Sciences*, 23:107–124, 1 2019. ISSN 16077938. doi: 10.5194/hess-23-107-2019.

N. Caine. The rainfall intensity-duration control of shallow landslides and debris flows. *Geografiska annaler: series A, physical geography*, 62(1-2): 23–27, 1980.

A. C. Callau Poduje and U. Haberlandt. Spatio-temporal synthesis of continuous precipitation series using vine copulas. *Water*, 10(7):862, 2018.

M. Cambou, M. Hofert, and C. Lemieux. Quasi-random numbers for copula models. *Statistics and Computing*, 27(5):1307–1329, 2017.

P. Camus, I. D. Haigh, A. A. Nasr, T. Wahl, S. E. Darby, and R. J. Nicholls. Regional analysis of multivariate compound coastal flooding potential around europe and environs: sensitivity analysis and spatial patterns. *Natural Hazards and Earth System Sciences*, 21(7), 2021.

S. H. Cannon, E. M. Boldt, J. L. Laber, J. W. Kean, and D. M. Staley. Rainfall intensity–duration thresholds for postfire debris-flow emergency-response planning. *Natural Hazards*, 59(1):209–236, 2011.

J. B. Cánovas, M. Stoffel, C. Corona, K. Schraml, A. Gobiet, S. Tani, F. Sinabell, S. Fuchs, and R. Kaitna. Debris-flow risk analysis in a managed torrent based on a stochastic life-cycle performance. *Science of the total environment*, 557:142–153, 2016.

P. Canuti, N. Casagli, M. Pellegrini, and G. Tosatti. Geo-hydrological hazards. In *Anatomy of an Orogen: the Apennines and adjacent mediterranean basins*, pages 513–532. Springer, 2001.

O. D. Cardona, M. K. Van Aalst, J. Birkmann, M. Fordham, G. Mc Gregor, P. Rosa, R. S. Pulwarty, E. L. F. Schipper, B. T. Sinh, H. Décamps, et al. Determinants of risk: exposure and vulnerability. In *Managing the risks of extreme events and disasters to advance climate change adaptation: special report of the intergovernmental panel on climate change*, pages 65–108. Cambridge University Press, 2012.

J. Cepeda, K. Höeg, and F. Nadim. Landslide-triggering rainfall thresholds: a conceptual framework. *Quarterly Journal of Engineering Geology and Hydrogeology*, 43(1):69–84, 2010.

T. Chau, S. Young, and S. Redekop. Managing variability in the summary and comparison of gait data. *Journal of neuroengineering and rehabilitation*, 2(1):1–20, 2005.

H. Chen, S. Zhang, M. Peng, and L. M. Zhang. A physically-based multi-hazard risk assessment platform for regional rainfall-induced slope failures and debris flows. *Engineering Geology*, 203:15–29, 2016.

C. Chien-Yuan, C. Tien-Chien, Y. Fan-Chieh, Y. Wen-Hui, and T. Chun-Chieh. Rainfall duration and debris-flow initiated studies for real-time monitoring. *Environmental Geology*, 47(5):715–724, 2005.

H. W. Coleman and W. G. Steele. *Experimentation, validation, and uncertainty analysis for engineers*. John Wiley & Sons, 2018.

S. Coles, J. Bawa, L. Trenner, and P. Dorazio. *An introduction to statistical modeling of extreme values*, volume 208. Springer, 2001.

S. G. Coles. Regional modelling of extreme storms via max-stable processes. *Journal of the Royal Statistical Society: Series B (Methodological)*, 55(4): 797–816, 1993.

D. Cooley and S. R. Sain. Spatial hierarchical modeling of precipitation extremes from a regional climate model. *Journal of agricultural, biological, and environmental statistics*, 15(3):381–402, 2010.

D. Cooley, D. Nychka, and P. Naveau. Bayesian spatial modeling of extreme precipitation return levels. *Journal of the American Statistical Association*, 102(479):824–840, 2007.

T. H. Cormen, C. E. Leiserson, R. L. Rivest, and C. Stein. *Introduction to algorithms*. MIT press, 2009.

CRED and UNISDR. Economic losses, poverty & disasters, 2018.

C. Czado. Pair-copula constructions of multivariate copulas. In *Copula theory and its applications*, pages 93–109. Springer, 2010.

C. Czado, U. Schepsmeier, and A. Min. Maximum likelihood estimation of mixed c-vines with application to exchange rates. *Statistical Modelling*, 16:229–255, 2012. doi: 10.1177/1471082X1101200302.

N. R. Dalezios. *Environmental hazards methodologies for risk assessment and management*. IWA Publishing, 2017.

R. Dave, S. S. Subramanian, and U. Bhatia. Extreme precipitation induced concurrent events trigger prolonged disruptions in regional road networks. *Environmental Research Letters*, 16:104050, 10 2021. ISSN 1748-9326. doi: 10.1088/1748-9326/AC2D67.

A. C. Davison and R. L. Smith. Models for exceedances over high thresholds. *Journal of the Royal Statistical Society: Series B (Methodological)*, 52(3): 393–425, 1990.

R. J. Dawson, T. Ball, J. Werritty, A. Werritty, J. W. Hall, and N. Roche. Assessing the effectiveness of non-structural flood management measures in the thames estuary under conditions of socio-economic and environmental change. *Global Environmental Change*, 21(2):628–646, 2011.

S. De Angeli, B. D. Malamud, L. Rossi, F. E. Taylor, E. Trasforini, and R. Rudari. A multi-hazard framework for spatial-temporal impact analysis. *International Journal of Disaster Risk Reduction*, page 102829, 2022.

C. De Michele, G. Salvadori, M. Canossi, A. Petaccia, and R. Rosso. Bivariate statistical approach to check adequacy of dam spillway. *Journal of Hydrologic Engineering*, 10(1):50–57, 2005.

M. L. Delignette-Muller and C. Dutang. fitdistrplus: An R package for fitting distributions. *Journal of statistical software*, 64:1–34, 2015.

J. Dißmann, E. C. Brechmann, C. Czado, and D. Kurowicka. Selecting and estimating regular vine copulae and application to financial returns. *Computational Statistics and Data Analysis*, 59:52–69, 3 2013. ISSN 01679473. doi: 10.1016/j.csda.2012.08.010.

C. A. Doswell III, R. Davies-Jones, and D. L. Keller. On summary measures of skill in rare event forecasting based on contingency tables. *Weather and forecasting*, 5(4):576–585, 1990.

F. Dottori, P. Salamon, A. Bianchi, L. Alfieri, F. A. Hirpa, and L. Feyen. Development and evaluation of a framework for global flood hazard mapping. *Advances in water resources*, 94:87–102, 2016.

C. A. Dowling and P. M. Santi. Debris flows and their toll on human life: a global analysis of debris-flow fatalities from 1950 to 2011. *Natural hazards*, 71(1):203–227, 2014.

N. V. Dung, B. Merz, A. Bárdossy, and H. Apel. Handling uncertainty in bivariate quantile estimation–An application to flood hazard analysis in the Mekong Delta. *Journal of Hydrology*, 527:704–717, 2015.

F. Durante and C. Sempi. *Principles of copula theory*, volume 474. CRC press Boca Raton, 2016.

F. Durante, E. P. Klement, and J. J. Quesada-Molina. Bounds for trivariate copulas with given bivariate marginals. *Journal of Inequalities and Applications*, 2008:1–9, 2008.

F. Durante, J. Fernández-Sánchez, and R. Pappadà. Copulas, diagonals, and tail dependence. *Fuzzy Sets and Systems*, 264:22–41, 4 2015. ISSN 0165-0114. doi: 10.1016/J.FSS.2014.03.014.

A. V. Dyrrdal, A. Lenkoski, T. L. Thorarinsdottir, and F. Stordal. Bayesian hierarchical modeling of extreme hourly precipitation in norway. *Environmetrics*, 26(2):89–106, 2015.

M. W. Fagerland, S. Lydersen, and P. Laake. *Statistical analysis of contingency tables*. Chapman and Hall/CRC, 2017.

G. Formetta, F. Marra, E. Dallan, M. Zaramella, and M. Borga. Differential orographic impact on sub-hourly, hourly, and daily extreme precipitation. *Advances in Water Resources*, 159:104085, 2022.

G. Frahm, M. Junker, and R. Schmidt. Estimating the tail-dependence coefficient: properties and pitfalls. *Insurance: mathematics and Economics*, 37(1):80–100, 2005.

P. Frattini, G. Crosta, and R. Sosio. Approaches for defining thresholds and return periods for rainfall-triggered shallow landslides. *Hydrological Processes: An International Journal*, 23(10):1444–1460, 2009.

E. W. Frees and E. A. Valdez. Understanding relationships using copulas. *North American Actuarial Journal*, 2:1–25, 1 1998. ISSN 10920277. doi: 10.1080/10920277.1998.10595667.

S. Fuchs, M. Keiler, S. Sokratov, and A. Shnyparkov. Spatiotemporal dynamics: the need for an innovative approach in mountain hazard risk management. *Natural hazards*, 68(3):1217–1241, 2013.

V. Gallina, S. Torresan, A. Critto, A. Sperotto, T. Glade, and A. Marcomini. A review of multi-risk methodologies for natural hazards: Consequences and challenges for a climate change impact assessment. *Journal of Environmental Management*, 168:123–132, 3 2016. ISSN 0301-4797. doi: 10.1016/J.JENVMAN.2015.11.011.

C. Gao, X. Guan, M. J. Booij, Y. Meng, and Y.-P. Xu. A new framework for a multi-site stochastic daily rainfall model: Coupling a univariate markov chain model with a multi-site rainfall event model. *Journal of Hydrology*, 598:126478, 2021.

M. Garcin, D. Guegan, and B. Hassani. A novel multivariate risk measure: the Kendall VaR, 2018.

S. L. Gariano, M. T. Brunetti, G. Iovine, M. Melillo, S. Peruccacci, O. Terranova, C. Vennari, and F. Guzzetti. Calibration and validation of rainfall thresholds for shallow landslide forecasting in Sicily, southern Italy. *Geomorphology*, 228:653–665, 2015.

S. L. Gariano, M. Melillo, S. Peruccacci, and M. T. Brunetti. How much does the rainfall temporal resolution affect rainfall thresholds for landslide triggering? *Natural Hazards*, 2020. ISSN 15730840.

C. Genest and A.-C. Favre. Everything you always wanted to know about copula modeling but were afraid to ask. *Journal of Hydrologic Engineering*, 12:347–368, 7 2007. ISSN 1084-0699. doi: 10.1061/(ASCE)1084-0699(2007)12:4(347).

C. Genest and L.-P. Rivest. Statistical inference procedures for bivariate archimedean copulas. *Journal of the American Statistical Association*, 88:1034, 9 1993. ISSN 01621459. doi: 10.2307/2290796.

U. Germann, G. Galli, M. Boscacci, and M. Bolliger. Radar precipitation measurement in a mountainous region. *Quarterly Journal of the Royal Meteorological Society: A journal of the atmospheric sciences, applied meteorology and physical oceanography*, 132(618):1669–1692, 2006.

T. Ghizzoni, G. Roth, and R. Rudari. Multivariate skew-t approach to the design of accumulation risk scenarios for the flooding hazard. *Advances in Water Resources*, 33:1243–1255, 10 2010. ISSN 0309-1708. doi: 10.1016/J.ADVWATRES.2010.08.003.

R. Giannecchini. Rainfall triggering soil slips in the southern apuan alps (tuscany, italy). *Advances in Geosciences*, 2:21–24, 2005.

R. Giannecchini, Y. Galanti, G. D. Avanzi, and M. Barsanti. Probabilistic rainfall thresholds for triggering debris flows in a human-modified landscape. *Geomorphology*, 257:94–107, 2016.

J. C. Gill and B. D. Malamud. Hazard interactions and interaction networks (cascades) within multi-hazard methodologies. *Earth System Dynamics*, 7(3):659–679, 2016.

E. Gioia, T. Carone, and F. Marincioni. Rainfall and land use empirically coupled to forecast landslides in the Esino river basin, central Italy. *Natural Hazards and Earth System Sciences*, 15(6):1289–1295, 2015.

L. Giovannini, S. Davolio, M. Zaramella, D. Zardi, and M. Borga. Multimodel convection-resolving simulations of the october 2018 vaia storm over northeastern italy. *Atmospheric Research*, 253:105455, 2021.

D. Godschalk, C. C. Bohl, T. Beatley, P. Berke, D. Brower, and E. J. Kaiser. *Natural hazard mitigation: Recasting disaster policy and planning*. Island press, 1999.

B. Graler, M. J. V. D. Berg, S. Vandenberghe, A. Petroselli, S. Grimaldi, B. D. Baets, and N. E. Verhoest. Multivariate return periods in hydrology: A critical and practical review focusing on synthetic design hydrograph estimation. *Hydrology and Earth System Sciences*, 17:1281–1296, 2013. ISSN 10275606. doi: 10.5194/hess-17-1281-2013.

F. Guzzetti, S. Peruccacci, M. Rossi, and C. P. Stark. Rainfall thresholds for the initiation of landslides in central and southern Europe. *Meteorology and Atmospheric Physics*, 98:239–267, 12 2007. ISSN 01777971.

F. Guzzetti, S. Peruccacci, M. Rossi, and C. P. Stark. The rainfall intensity–duration control of shallow landslides and debris flows: an update. *Landslides*, 5(1):3–17, 2008.

L. Håkanson. The role of characteristic coefficients of variation in uncertainty and sensitivity analyses, with examples related to the structuring of lake eutrophication models. *Ecological modelling*, 131(1):1–20, 2000.

X. Han, R. Mehrotra, and A. Sharma. Measuring the spatial connectivity of extreme rainfall. *Journal of Hydrology*, 590:125510, 2020.

A. Hanssen and W. Kuipers. *On the relationship between the frequency of rain and various meteorological parameters: with reference to the problem of objective forecasting*. Staatsdrukkerij-en Uitgeverijbedrijf, 1965.

Z. Hao and V. P. Singh. Review of dependence modeling in hydrology and water resources. *Progress in Physical Geography*, 40(4):549–578, 2016.

Z. Hao, V. P. Singh, and F. Hao. Compound extremes in hydroclimatology: a review. *Water*, 10(6):718, 2018.

J. C. Helton, J. D. Johnson, C. J. Sallaberry, and C. B. Storlie. Survey of sampling-based methods for uncertainty and sensitivity analysis. *Reliability Engineering and System Safety*, 91:1175–1209, 10 2006. ISSN 09518320.

J. Hirschberg, A. Badoux, B. W. McArdell, E. Leonarduzzi, and P. Molnar. Evaluating methods for debris-flow prediction based on rainfall in an Alpine catchment. *Natural Hazards and Earth System Sciences*, 21(9): 2773–2789, 2021.

E. Hofer. *The Uncertainty Analysis of Model Results*. Springer International Publishing, 2018.

M. Hofert, I. Kojadinovic, M. Maechler, J. Yan, M. M. Maechler, and M. Suggests. *Package 'copula'. Multivariate Dependence with Copulas*, 2020. URL `https://cran.r-project.org/web/packages/copula/index.html`.

J. Huang, T. W. J. v. Asch, C. Wang, and Q. Li. Study on the combined threshold for gully-type debris flow early warning. *Natural hazards and earth system sciences*, 19(1):41–51, 2019.

K. Huang, L. Chen, J. Zhou, J. Zhang, and V. P. Singh. Flood hydrograph coincidence analysis for mainstream and its tributaries. *Journal of Hydrology*, 565:341–353, 10 2018. ISSN 00221694. doi: 10.1016/j.jhydrol.2018.08.007.

J. Huebl and G. Fiebiger. Debris-flow mitigation measures. In *Debris-flow hazards and related phenomena*, pages 445–487. Springer, 2005.

O. Hungr, S. Evans, M. Bovis, and J. Hutchinson. A review of the classification of landslides of the flow type. *Environmental & Engineering Geoscience*, 8(1), 2002.

C. Iadanza, M. Rianna, D. Orlando, L. Ubertini, and F. Napolitano. Identification of independent storm events: Seasonal and spatial variability of times between storms in Alpine area. In *AIP Conference Proceedings*, volume 1558, pages 1689–1692. American Institute of Physics, 2013.

C. Iadanza, A. Trigila, and F. Napolitano. Identification and characterization of rainfall events responsible for triggering of debris flows and shallow landslides. *Journal of Hydrology*, 541:230–245, 10 2016. ISSN 00221694.

R. M. Iverson. The physics of debris flows. *Reviews of geophysics*, 35(3): 245–296, 1997.

R. M. Iverson. Debris flows: behaviour and hazard assessment. *Geology today*, 30(1):15–20, 2014.

M. Jakob, T. Owen, and T. Simpson. A regional real-time debris-flow warning system for the District of North Vancouver, Canada. *Landslides*, 9 (2):165–178, 2012a.

M. Jakob, T. Owen, and T. Simpson. A regional real-time debris-flow warning system for the District of North Vancouver, Canada. *Landslides*, 9 (2):165–178, 2012b.

M. Jakob, D. Stein, and M. Ulmi. Vulnerability of buildings to debris flow impact. *Natural hazards*, 60(2):241–261, 2012c.

F. Jalayer, G. T. Aronica, A. Recupero, S. Carozza, and G. Manfredi. Debris flow damage incurred to buildings: an in situ back analysis. *Journal of Flood Risk Management*, 11:S646–S662, 2018.

R. Jane, L. Cadavid, J. Obeysekera, and T. Wahl. Multivariate statistical modelling of the drivers of compound flood events in south florida. *Natural Hazards and Earth System Sciences*, 20:2681–2699, 10 2020. ISSN 1684-9981. doi: 10.5194/nhess-20-2681-2020.

N. Javidan, A. Kavian, H. R. Pourghasemi, C. Conoscenti, Z. Jafarian, and J. Rodrigo-Comino. Evaluation of multi-hazard map produced using MaxEnt machine learning technique. *Scientific Reports 2021 11:1*, 11: 1–20, 3 2021. ISSN 2045-2322. doi: 10.1038/s41598-021-85862-7.

H. Joe. Families of m-variate distributions with given margins and m (m-1)/2 bivariate dependence parameters. *Lecture Notes-Monograph Series*, pages 120–141, 1996.

H. Joe. *Multivariate models and multivariate dependence concepts*. CRC press, 1997.

H. Joe. *Dependence modeling with copulas*. CRC press, 2014.

H. Joe and D. Kurowicka, editors. *Dependence modeling: vine copula handbook*. World Scientific, 2011.

I. T. Jolliffe and D. B. Stephenson. *Forecast verification: a practitioner's guide in atmospheric science*. John Wiley & Sons, 2012.

S. N. Jonkman and I. Kelman. An analysis of the causes and circumstances of flood disaster deaths. *Disasters*, 29(1):75–97, 2005.

G. Jordanova, S. L. Gariano, M. Melillo, S. Peruccacci, M. T. Brunetti, and M. Jemec Auflič. Determination of empirical rainfall thresholds for shallow landslides in Slovenia using an automatic tool. *Water*, 12(5):1449, 2020.

V. V. Kharin and F. W. Zwiers. On the ROC score of probability forecasts. *Journal of Climate*, 16(24):4145–4150, 2003.

B. J. Kim, S. Jeong, and J.-B. Chung. Research trends in vulnerability studies from 2000 to 2019: Findings from a bibliometric analysis. *International Journal of Disaster Risk Reduction*, 56:102141, 2021.

M. Kuller, K. Schoenholzer, and J. Lienert. Creating effective flood warnings: A framework from a critical review. *Journal of Hydrology*, 602: 126708, 11 2021. ISSN 0022-1694. doi: 10.1016/J.JHYDROL.2021.126708.

Z. W. Kundzewicz. Non-structural flood protection and sustainability. *http://dx.doi.org/10.1080/02508060208686972*, 27:3–13, 2009. ISSN 02508060. doi: 10.1080/02508060208686972.

D. Kurowicka and R. M. Cooke. *Uncertainty analysis with high dimensional dependence modelling*. John Wiley & Sons, 2006.

E. W. Lane. Progress report on studies on the design of stable channels by the bureau of reclamation. In *Proceedings of the American Society of Civil Engineers*, volume 79, pages 1–31. ASCE, 1953.

M. Lazzari, M. Piccarreta, and D. Capolongo. Landslide triggering and local rainfall thresholds in Bradanic Foredeep, Basilicata region (Southern Italy). In *Landslide science and practice*, pages 671–677. Springer, 2013.

P. D. Le, M. Leonard, and S. Westra. Modeling spatial dependence of rainfall extremes across multiple durations. *Water Resources Research*, 54:2233–2248, 3 2018. ISSN 1944-7973. doi: 10.1002/2017WR022231.

P. D. Le, M. Leonard, and S. Westra. Spatially dependent flood probabilities to support the design of civil infrastructure systems. *Hydrology and Earth System Sciences*, 23(11):4851–4867, 2019.

E. Leonarduzzi and P. Molnar. Deriving rainfall thresholds for landsliding at the regional scale: daily and hourly resolutions, normalisation, and antecedent rainfall. *Natural Hazards and Earth System Sciences*, 20(11): 2905–2919, 2020.

E. Leonarduzzi, P. Molnar, and B. W. McArdell. Predictive performance of rainfall thresholds for shallow landslides in Switzerland from gridded daily data. *Water Resources Research*, 53(8):6612–6625, 2017.

T.-T. Li, R.-Q. Huang, and X.-J. Pei. Variability in rainfall threshold for debris flow after wenchuan earthquake in gaochuan river watershed, southwest china. *Natural Hazards*, 82(3):1967–1980, 2016.

B. Liu, Y. L. Siu, and G. Mitchell. Hazard interaction analysis for multi-hazard risk assessment: a systematic classification based on hazard-forming environment. *Natural Hazards and Earth System Sciences*, 16 (2):629–642, 2016.

W. Liu, S. He, and C. Ouyang. Two-dimensional dynamics simulation of two-phase debris flow. *Acta Geologica Sinica-English Edition*, 91(5):1873–1883, 2017.

G. D. Luca and G. Rivieccio. Multivariate tail dependence coefficients for archimedean copulae. In *Advanced statistical methods for the analysis of large data-sets*, pages 287–296. Springer, 2012.

T. Lux and A. Papapantoleon. Improved fréchet–hoeffding bounds on d-copulas and applications in model-free finance. *https://doi.org/10.1214/17-AAP1292*, 27:3633–3671, 12 2017. ISSN 1050-5164. doi: 10.1214/17-AAP1292.

P. d. C. Luz Barcellos, M. S. Da Costa, M. Cataldi, and C. A. P. Soares. Management of non-structural measures in the prevention of flash floods: a case study in the city of duque de caxias, state of rio de janeiro, brazil. *Natural Hazards*, 89(1):313–330, 2017.

E. Maidl and M. Buchecker. Raising risk preparedness by flood risk communication. *Natural Hazards and Earth System Sciences*, 15(7):1577–1595, 2015.

M. Marani and M. Ignaccolo. A metastatistical approach to rainfall extremes. *Advances in Water Resources*, 79:121–126, 2015.

L. Marchi, M. T. Brunetti, M. Cavalli, and S. Crema. Debris-flow volumes in northeastern italy: Relationship with drainage area and size probability. *Earth Surface Processes and Landforms*, 44(4):933–943, 2019.

S. Marino, I. B. Hogue, C. J. Ray, and D. E. Kirschner. A methodology for performing global uncertainty and sensitivity analysis in systems biology. *Journal of Theoretical Biology*, 254:178–196, 9 2008. ISSN 00225193.

F. Marra. Rainfall thresholds for landslide occurrence: systematic underestimation using coarse temporal resolution data. *Natural Hazards*, 95(3): 883–890, 2019.

F. Marra, E. I. Nikolopoulos, J. D. Creutin, and M. Borga. Radar rainfall estimation for the identification of debris-flow occurrence thresholds. *Journal of Hydrology*, 519:1607–1619, 11 2014. ISSN 00221694.

F. Marra, E. I. Nikolopoulos, J. D. Creutin, and M. Borga. Space–time organization of debris flows-triggering rainfall and its effect on the identification of the rainfall threshold relationship. *Journal of Hydrology*, 541: 246–255, 10 2016. ISSN 00221694.

F. Marra, E. I. Nikolopoulos, E. N. Anagnostou, and E. Morin. Metastatistical extreme value analysis of hourly rainfall from short records: Estimation of high quantiles and impact of measurement errors. *Advances in water resources*, 117:27–39, 2018.

F. Marra, D. Zoccatelli, M. Armon, and E. Morin. A simplified mev formulation to model extremes emerging from multiple nonstationary underlying processes. *Advances in water resources*, 127:280–290, 2019.

F. Marra, M. Borga, and E. Morin. A unified framework for extreme subdaily precipitation frequency analyses based on ordinary events. *Geophysical Research Letters*, 47(18):e2020GL090209, 2020.

F. Marra, M. Armon, and E. Morin. Coastal and orographic effects on extreme precipitation revealed by weather radar observations. *Hydrology and Earth System Sciences*, 26:1439–1458, 3 2022. ISSN 1607-7938. doi: 10.5194/HESS-26-1439-2022.

J. S. Marshall and W. Palmer. The distribution of raindrops with size. *J. Meteorol.*, 5:165–166, 1948.

M. Martinengo, A. Ziantoni, F. Lazzeri, G. Rosatti, and R. Rigon. A practitioners' view on the application of the water framework directive and the Floods Directive in Italy. In *Water Law, Policy and Economics in Italy*, pages 369–393. Springer, 2021a.

M. Martinengo, D. Zugliani, and G. Rosatti. Uncertainty analysis of a rainfall threshold estimate for stony debris flow based on the backward dynamical approach. *Natural Hazards and Earth System Sciences*, 21(6): 1769–1784, 2021b.

M. Martinengo, D. Zugliani, and G. Rosatti. Validation and potential forecast use of a debris-flow rainfall threshold calibrated with the backward dynamical approach. Manuscript submitted for publication, 2022.

M. D. McKay, R. J. Beckman, and W. J. Conover. A comparison of three methods for selecting values of input variables in the analysis of output from a computer code. *Technometrics*, 42(1):55–61, 2000.

H. Mees, A. Crabbé, M. Alexander, M. Kaufmann, S. Bruzzone, L. Lévy, and J. Lewandowski. Coproducing flood risk management through citizen involvement: insights from cross-country comparison in europe. *Ecology and Society*, 21(3), 2016.

F. Michiels, I. Koch, and A. D. Schepper. A new method for the construction of bivariate archimedean copulas based on the λ function. *Communications in Statistics-Theory and Methods*, 40:2670–2679, 2011. ISSN 0361-0926. doi: 10.1080/03610926.2010.489180.

X. Ming, Q. Liang, R. Dawson, X. Xia, and J. Hou. A quantitative multi-hazard risk assessment framework for compound flooding considering hazard inter-dependencies and interactions. *Journal of Hydrology*, 607: 127477, 4 2022. ISSN 0022-1694. doi: 10.1016/J.JHYDROL.2022.127477.

A. Miniussi and M. Marani. Estimation of daily rainfall extremes through the metastatistical extreme value distribution: Uncertainty minimization and implications for trend detection. *Water Resources Research*, 56(7): e2019WR026535, 2020.

A. Miniussi and F. Marra. Estimation of extreme daily precipitation return levels at-site and in ungauged locations using the simplified mev approach. *Journal of Hydrology*, 603:126946, 2021.

E. Mondino, A. Scolobig, M. Borga, and G. Di Baldassarre. The role of experience and different sources of knowledge in shaping flood risk awareness. *Water*, 12(8):2130, 2020.

K. Mostbauer, R. Kaitna, D. Prenner, and M. Hrachowitz. The temporally varying roles of rainfall, snowmelt and soil moisture for debris flow initiation in a snow-dominated system. *Hydrology and Earth System Sciences*, 22(6):3493–3513, 2018.

R. B. Mudashiru, N. Sabtu, I. Abustan, and W. Balogun. Flood hazard mapping methods: A review. *Journal of Hydrology*, 603:126846, 2021.

P. Mujumdar et al. Dependence structure of urban precipitation extremes. *Advances in Water Resources*, 121:206–218, 2018.

S. Nadarajah, E. Afuecheta, and S. Chan. A compendium of copulas. *Statistica*, 77(4):279–328, 2017.

T. Nagler and T. Vatter. *Package 'rvinecopulib'. High Performance Algorithms for Vine Copula Modeling*, 2021. URL `https://cran.r-project.org/web/packages/rvinecopulib/index.html`.

R. B. Nelsen. *An introduction to copulas*. Springer Science & Business Media, 2006.

R. B. Nelsen, J. J. Quesada-Molina, J. A. Rodriguez-Lallena, and M. Úbeda-Flores. Distribution functions of copulas: a class of bivariate probability integral transforms. *Statistics & Probability Letters*, 54(3):277–282, 2001.

R. B. Nelsen, J. J. Quesada-Molina, J. A. Rodrıguez-Lallena, and M. Úbeda-Flores. Kendall distribution functions. *Statistics & probability letters*, 65 (3):263–268, 2003.

E. I. Nikolopoulos, S. Crema, L. Marchi, F. Marra, F. Guzzetti, and M. Borga. Impact of uncertainty in rainfall estimation on the identification of rainfall thresholds for debris flow occurrence. *Geomorphology*, 221:286–297, 2014.

W. L. Oberkampf, J. C. Helton, C. A. Joslyn, S. F. Wojtkiewicz, and S. Ferson. Challenge problems: uncertainty in system response given uncertain parameters. *Reliability Engineering & System Safety*, 85(1-3):11–19, 2004.

A. B. Owen. Quasi-monte carlo sampling. *Monte Carlo Ray Tracing: Siggraph*, pages 69–88, 2003.

M. Pal, M. M. Ali, and J. Woo. Exponentiated weibull distribution. *Statistica*, 66(2):139–147, 2006.

G. Paliaga, F. Luino, L. Turconi, F. Marincioni, and F. Faccini. Exposure to geo-hydrological hazards of the metropolitan area of genoa, italy: A multi-temporal analysis of the bisagno stream. *Sustainability*, 12(3):1114, 2020.

H.-L. Pan, Y.-J. Jiang, J. Wang, and G.-Q. Ou. Rainfall threshold calculation for debris flow early warning in areas with scarcity of data. *Natural Hazards and Earth System Sciences*, 18(5):1395–1409, 2018.

K. Papagiannaki, M. Diakakis, V. Kotroni, K. Lagouvardos, and E. Andreadakis. Hydrogeological and climatological risks perception in a multi-hazard environment: The case of Greece. *Water 2019, Vol. 11, Page 1770*, 11:1770, 8 2019a. ISSN 2073-4441. doi: 10.3390/W11091770.

K. Papagiannaki, V. Kotroni, K. Lagouvardos, and G. Papagiannakis. How awareness and confidence affect flood-risk precautionary behavior of greek citizens: The role of perceptual and emotional mechanisms. *Natural Hazards and Earth System Sciences*, 19(7):1329–1346, 2019b.

R. Pappadà. *Copula-based measures of tail dependence with applications*. PhD thesis, Università degli Studi di Padova, 2014.

C. S. Peirce. The numerical measure of the success of predictions. *Science*, (93):453–454, 1884.

D. Peres and A. Cancelliere. Derivation and evaluation of landslide-triggering thresholds by a monte carlo approach. *Hydrology and Earth System Sciences*, 18(12):4913–4931, 2014.

D. J. Peres and A. Cancelliere. Comparing methods for determining landslide early warning thresholds: potential use of non-triggering rainfall for locations with scarce landslide data availability. *Landslides*, pages 1–13, 2021.

D. J. Peres, A. Cancelliere, R. Greco, and T. A. Bogaard. Influence of uncertain identification of triggering rainfall on the assessment of landslide early warning thresholds. *Natural Hazards and Earth System Sciences*, 18(2):633–646, 2018.

S. Peruccacci, M. T. Brunetti, S. Luciani, C. Vennari, and F. Guzzetti. Lithological and seasonal control on rainfall thresholds for the possible initiation of landslides in central Italy. *Geomorphology*, 139:79–90, 2012.

G. Pesaro, M. Mendoza, G. Minucci, and S. Menoni. Cost-benefit analysis for non-structural flood risk mitigation measures: Insights and lessons learnt from a real case study. In *Safety and Reliability–Safe Societies in a Changing World*, pages 109–118. CRC Press, 2018.

O. Petrucci and M. Polemio. The use of historical data for the characterisation of multiple damaging hydrogeological events. *Natural Hazards and Earth System Sciences*, 3(1/2):17–30, 2003.

O. Petrucci, L. Aceto, C. Bianchi, V. Bigot, R. Brázdil, S. Pereira, A. Kahraman, Ö. Kılıç, V. Kotroni, M. C. Llasat, et al. Flood fatalities in Europe, 1980–2018: Variability, features, and lessons to learn. *Water*, 11(8):1682, 2019.

S. Piccolroaz, G. Bertoldi, M. Borga, A. Casonato, L. Marchi, T. Michelini, G. Rosatti, and R. Valentinotti. Extreme events and aging of defence works challenge the definition of residual scenarios for debris-flow hazard assessment: the case of the Rotiano creek (Province of Trento, Italy). In A. International Research Society INTERPRAEVENT, Klagenfurt, editor, *INTERPRAEVENT 2021 – Extended Abstracts*, 2021.

L. Piciullo, S. L. Gariano, M. Melillo, M. T. Brunetti, S. Peruccacci, F. Guzzetti, and M. Calvello. Definition and performance of a threshold-based regional early warning model for rainfall-induced landslides. *Landslides*, 14(3):995–1008, 2017.

M. Pirulli and G. Sorbino. Assessing potential debris flow runout: a comparison of two simulation models. *Natural Hazards and Earth System Sciences*, 8(4):961–971, 2008.

M. Ponziani, P. Pogliotti, H. Stevenin, and S. M. Ratto. Debris-flow Indicator for an early warning system in the Aosta valley region. *Natural Hazards*, 104(2):1819–1839, 2020.

J. P. Prancevic and M. P. Lamb. Unraveling bed slope from relative roughness in initial sediment motion. *Journal of Geophysical Research: Earth Surface*, 120(3):474–489, 2015.

S. P. Pudasaini. A general two-phase debris flow model. *Journal of Geophysical Research: Earth Surface*, 117(F3), 2012.

R Core Team. *R: A Language and Environment for Statistical Computing*. R Foundation for Statistical Computing, Vienna, Austria, 2013. URL `http://www.R-project.org/`.

M. Reghezza-Zitt and S. Rufat. Disentangling the range of responses to threats, hazards and disasters. vulnerability, resilience and adaptation in question. *Cybergeo: European Journal of Geography*, 2019.

P. J. Restrepo-Posada and P. S. Eagleson. Identification of independent rainstorms. *Journal of Hydrology*, 55(1-4):303–319, 1982.

P. Revellino, L. Guerriero, N. Mascellaro, F. Fiorillo, G. Grelle, G. Ruzza, and F. M. Guadagno. Multiple effects of intense meteorological events in the benevento province, southern italy. *Water*, 11(8):1560, 2019.

G. Rosatti and L. Begnudelli. A closure-independent generalized roe solver for free-surface, two-phase flows over mobile bed. *Journal of Computational Physics*, 255:362–383, 2013.

G. Rosatti, N. Zorzi, L. Begnudelli, and A. Armanini. Evaluation of the TRENT2D Model Capabilities to Reproduce and Forecast Debris-Flow Deposition Patterns Through a Back Analysis of a Real Event. In *Engineering Geology for Society and Territory-Volume 2*, pages 1629–1633. Springer, 2015.

G. Rosatti, N. Zorzi, D. Zugliani, S. Piffer, and A. Rizzi. A Web Service ecosystem for high-quality, cost-effective debris-flow hazard assessment. *Environmental modelling & software*, 100:33–47, 2018.

G. Rosatti, D. Zugliani, M. Pirulli, and M. Martinengo. A new method for evaluating stony debris flow rainfall thresholds: the Backward Dynamical Approach. *Heliyon*, 5, 6 2019. ISSN 24058440.

M. Rossi, S. Luciani, D. Valigi, D. Kirschbaum, M. Brunetti, S. Peruccacci, and F. Guzzetti. Statistical approaches for the definition of landslide rainfall thresholds and their uncertainty using rain gauge and satellite data. *Geomorphology*, 285:16–27, 2017.

M. Sadegh, H. Moftakhari, H. V. Gupta, E. Ragno, O. Mazdiyasni, B. Sanders, R. Matthew, and A. AghaKouchak. Multihazard scenarios for analysis of compound extreme events. *Geophysical Research Letters*, 45:5470–5480, 6 2018. ISSN 0094-8276. doi: 10.1029/2018GL077317.

G. Salvadori, C. D. Michele, and F. Durante. On the return period and design in a multivariate framework. *Hydrology and Earth System Sciences*, 15:3293–3305, 2011. ISSN 10275606. doi: 10.5194/hess-15-3293-2011.

G. Salvadori, F. Durante, and C. D. Michele. Multivariate return period calculation via survival functions. *Water Resources Research*, 49:2308–2311, 4 2013. ISSN 00431397. doi: 10.1002/wrcr.20204.

G. Salvadori, F. Durante, C. D. Michele, M. Bernardi, and L. Petrella. A multivariate copula-based framework for dealing with hazard scenarios and failure probabilities. *Water Resources Research*, 52:3701–3721, 5 2016. ISSN 19447973. doi: 10.1002/2015WR017225.

H. Schellander, A. Lieb, and T. Hell. Error structure of metastatistical and generalized extreme value distributions for modeling extreme rainfall in austria. *Earth and Space Science*, 6(9):1616–1632, 2019.

U. Schepsmeier, J. Stoeber, E. C. Brechmann, B. Graeler, T. Nagler, T. Erhardt, C. Almeida, A. Min, C. Czado, M. Hofmann, et al. Package 'vinecopula'. *R package version*, 2(5), 2015.

U. Schepsmeier, J. Stoeber, E. C. Brechmann, B. Graeler, T. Nagler, T. Erhardt, C. Almeida, A. Min, C. Czado, M. Hofmann, et al. *Package 'vinecopula'. Statistical Inference of Vine Copulas*, 2021. URL `https://cran.r-project.org/web/packages/VineCopula/index.html`.

E. M. Schliep, D. Cooley, S. R. Sain, and J. A. Hoeting. A comparison study of extreme precipitation from six different regional climate models via spatial hierarchical modeling. *Extremes*, 13(2):219–239, 2010.

I. S. Schwartz and D. M. Baer. Social validity assessments: Is current practice state of the art? *Journal of applied behavior analysis*, 24(2): 189–204, 1991.

S. Segoni, G. Rossi, A. Rosi, and F. Catani. Landslides triggered by rainfall: A semi-automated procedure to define consistent intensity–duration thresholds. *Computers & Geosciences*, 63:123–131, 2014.

S. Segoni, L. Piciullo, and S. L. Gariano. A review of the recent literature on rainfall thresholds for landslide occurrence. *Landslides*, 15:1483–1501, 8 2018. ISSN 16125118.

F. Serinaldi. A multisite daily rainfall generator driven by bivariate copula-based mixed distributions. *Journal of Geophysical Research: Atmospheres*, 114:10103, 5 2009. ISSN 2156-2202. doi: 10.1029/2008JD011258.

F. Serinaldi. Dismissing return periods! *Stochastic Environmental Research and Risk Assessment*, 29:1179–1189, 5 2015. ISSN 14363259. doi: 10.1007/s00477-014-0916-1.

F. Serinaldi, F. Lombardo, and C. G. Kilsby. All in order: Distribution of serially correlated order statistics with applications to hydrological extremes. *Advances in Water Resources*, 144:103686, 2020. doi: 10.1016/j.advwatres.2020.103686. URL `https://doi.org/10.1016/j.advwatres.2020.103686`.

P. Sharkey and H. C. Winter. A bayesian spatial hierarchical model for extreme precipitation in great britain. *Environmetrics*, 30(1):e2529, 2019.

C.-L. Shieh, Y. Chen, Y. Tsai, and J. Wu. ariability in rainfall threshold for debris flow after the Chi-Chi earthquake in central Taiwan, China. *International Journal of Sediment Research*, 24(2):177–188, 2009.

M. Sibuya et al. Bivariate extreme statistics. *Annals of the Institute of Statistical Mathematics*, 11(2):195–210, 1960.

B. W. Silverman. *Density estimation for statistics and data analysis*. Routledge, 2018.

S. P. Simonovic. Two new non-structural measures for sustainable management of floods, water international. *Water International*, 27:38–46, 2002. ISSN 1941-1707. doi: 10.1080/02508060208686976.

A. Sklar. Fonctions de répartition à n dimensions et leurs marges. *Publications de l'Institut Statistique de l'Universite de Paris*, 8:229–231, 1959.

D. M. Staley, J. W. Kean, S. H. Cannon, K. M. Schmidt, and J. L. Laber. Objective definition of rainfall intensity–duration thresholds for the initiation of post-fire debris flows in southern california. *Landslides*, 10(5): 547–562, 2013.

L. Stancanelli, S. Lanzoni, and E. Foti. Propagation and deposition of stony debris flows at channel confluences. *Water Resources Research*, 51 (7):5100–5116, 2015.

M. Staro minski-Uehara. How structural mitigation shapes risk perception and affects decision-making. *Disasters*, 45(1):46–66, 2021.

A. G. Stephenson, E. A. Lehmann, and A. Phatak. A max-stable process model for rainfall extremes at different accumulation durations. *Weather and Climate Extremes*, 13:44–53, 9 2016. ISSN 2212-0947. doi: 10.1016/J.WACE.2016.07.002.

T. Takahashi. Mechanical characteristics of debris flow. *Journal of the Hydraulics Division*, 104(8):1153–1169, 1978.

T. Takahashi. *Debris flow: mechanics, prediction and countermeasures.* Taylor & Francis, 2007.

T. Takahashi. A review of japanese debris flow research. *International Journal of Erosion Control Engineering*, 2(1):1–14, 2009.

T. Takahashi. *Debris flow: mechanics, prediction and countermeasures.* CRC press, 2014.

C. Tang, J. Zhu, W. Li, and J. Liang. Rainfall-triggered debris flows following the wenchuan earthquake. *Bulletin of Engineering Geology and the Environment*, 68(2):187–194, 2009.

A. Tavakol, V. Rahmani, and J. Harrington. Probability of compound climate extremes in a changing climate: A copula-based study of hot, dry, and windy events in the central united states. *Environmental Research Letters*, 15:104058, 10 2020. ISSN 17489326. doi: 10.1088/1748-9326/abb1ef.

J. Teng, A. J. Jakeman, J. Vaze, B. F. Croke, D. Dutta, and S. Kim. Flood inundation modelling: A review of methods, recent advances and uncertainty analysis. *Environmental modelling & software*, 90:201–216, 2017.

E. Thibaud, R. Mutzner, and A. C. Davison. Threshold modeling of extreme spatial rainfall. *Water resources research*, 49(8):4633–4644, 2013.

A. Tilloy, B. D. Malamud, H. Winter, and A. Joly-Laugel. Evaluating the efficacy of bivariate extreme modelling approaches for multi-hazard scenarios. *Natural Hazards and Earth System Sciences*, 20:2091–2117, 8 2020. ISSN 1684-9981. doi: 10.5194/nhess-20-2091-2020.

A. Trigila, C. Iadanza, B. Lastoria, M. Bussettini, and B. A. Dissesto idrogeologico in Italia: pericolosità e indicatori di rischio - Edizione 2021. ISPRA, Rapporti 356/2021, 2021.

H. Tsukahara. Semiparametric estimation in copula models. *Canadian Journal of Statistics*, 33(3):357–375, 2005.

R. Uijlenhoet. Raindrop size distributions and radar reflectivity-rain rate relationships for radar hydrology. *Hydrology and Earth System Sciences*, 5(4):615–627, 2001.

UNDRR. United Nations Office for Disaster Risk Reduction. Sendai Framework for Disaster Risk Reduction 2015 - 2030, 2015. URL `www.unisdr.org/files/43291_sendaiframeworkfordrren.pdf`.

UNISDR. Living with Risk. A global review of disaster reduction initiatives. United Nations Inter-Agency Secretariat of the International Strategy for Disaster Reduction, 2004. URL www.unisdr.org/files/657_lwr1.pdf.

K. Van der Heijden. *Scenarios: the art of strategic conversation.* John Wiley & Sons, 2005.

C. J. van Westen and S. Greiving. Multi-hazard risk assessment and decision making. *Environmental hazards methodologies for risk assessment and management*, 31, 2017.

S. Vandenberghe, N. Verhoest, C. Onof, and B. De Baets. A comparative copula-based bivariate frequency analysis of observed and simulated storm events: A case study on bartlett-lewis modeled rainfall. *Water Resources Research*, 47(7), 2011.

G. G. Venter et al. Tails of copulas. In *Proceedings of the Casualty Actuarial Society*, volume 89, pages 68–113, 2002.

E. Volpi and A. Fiori. Design event selection in bivariate hydrological frequency analysis. *Hydrological Sciences Journal*, 57:1506–1515, 11 2012. ISSN 0262-6667. doi: 10.1080/02626667.2012.726357.

E. Volpi, A. Fiori, S. Grimaldi, F. Lombardo, and D. Koutsoyiannis. Save hydrological observations! Return period estimation without data decimation. *Journal of Hydrology*, 571:782–792, 4 2019. ISSN 0022-1694. doi: 10.1016/J.JHYDROL.2019.02.017.

WEF. World Economic Forum. The Global Risk Report, 2019. URL www3.weforum.org/docs/WEF_Global_Risks_Report_2019.pdf.

W. Wiedermann and A. Von Eye. *Statistics and causality.* Wiley Online Library, 2016.

D. S. Wilks. *Statistical methods in the atmospheric sciences*, volume 100. Academic press, 2011.

M. Winter, J. Dent, F. Macgregor, P. Dempsey, A. Motion, and L. Shackman. Debris flow, rainfall and climate change in scotland. *Quarterly Journal of Engineering Geology and Hydrogeology*, 43(4):429–446, 2010.

R. Yu, R. Yang, C. Zhang, M. Špoljar, N. Kuczyńska-Kippen, and G. Sang. A vine copula-based modeling for identification of multivariate water pollution risk in an interconnected river system network. *Water*, 12:2741, 9 2020. ISSN 2073-4441. doi: 10.3390/w12102741.

S. J. Zhang, C. X. Xu, F. Q. Wei, K. H. Hu, H. Xu, L. Q. Zhao, and G. P. Zhang. A physics-based model to derive rainfall intensity-duration threshold for debris flow. *Geomorphology*, 351, 2 2020. ISSN 0169555X.

Y. Zhao, X. Meng, T. Qi, G. Chen, Y. Li, D. Yue, and F. Qing. Modeling the Spatial Distribution of Debris Flows and Analysis of the Controlling Factors: A Machine Learning Approach. *Remote Sensing*, 13(23):4813, 2021.

W. Zhou and C. Tang. Rainfall thresholds for debris flow initiation in the wenchuan earthquake-stricken area, southwestern china. *Landslides*, 11 (5):877–887, 2014.

S. Zhu, Z. Xu, X. Luo, C. Wang, and J. Wu. Assessing coincidence probability for extreme precipitation events in the jinsha river basin. *Theoretical and Applied Climatology*, 139:825–835, 1 2020. ISSN 14344483. doi: 10.1007/S00704-019-03009-1/FIGURES/6.

J. Zhuang, P. Cui, G. Wang, X. Chen, J. Iqbal, and X. Guo. Rainfall thresholds for the occurrence of debris flows in the Jiangjia Gully, Yunnan Province, China. *Engineering geology*, 195:335–346, 2015.

E. Zorzetto, G. Botter, and M. Marani. On the emergence of rainfall extremes from ordinary events. *Geophysical Research Letters*, 43(15):8076–8082, 2016.

Acknowledgements

First and foremost, I would like to thank Prof. Giorgio Rosatti for believing in me and giving me the opportunity of working on a topic that I'm passionate about. I also want to thank him for his advice and feedback and for allowing me to participate in several research projects. The collaboration with him made me grow personally and technically.

I would like to thank Prof. Riccardo Rigon e Prof. Luigi Fraccarollo for the advice they gave me and for the esteem they showed me.

I want to thank Prof. Marco Borga and Prof. Aldo Fiori who were the reviewers of this thesis. I am grateful to them for their observations and appreciation for my research work.

I would like to thank Francesco Marra and Prof. Giuseppe Formetta for their availability and advice that were significant to improve Chapter 4 of this thesis.

I thank Ripartizione Opere Idrauliche and Ufficio Idrografico, Provincia Autonoma di Bolzano (Italy), and Ufficio Previsioni e Pianificazione and Servizio Bacini Montani, Provincia Autonoma di Trento (Italy), for providing radar and debris-flow data.

I want to thank all the colleagues who have followed one another in the 407 bis office and who have supported me on this path. A special thanks to Daniel, a constant presence in the office (except early in the morning), for his valuable advice and ongoing support. A particular thanks to Stefania, my companion on this path. With her, I shared difficulties and satisfactions, anxiety (a lot!) and happiness, all accompanied by the shaking of her chair.

I would like to give special thanks to my old and new friends from Brescia, Trento and Parma for supporting me in the various phases of my PhD.

A huge thanks to my family for constant and unlimited support during these years.

A loving thanks to Paolo for always motivating me and helping me to continue the path even in the most difficult moments.

Finally, I want to thank my *bestiolina* to whom this work is dedicated.

Hydrogeological hazards are quite diffuse rainfall-induced phenomena that affect mountain regions and can severely impact these territories, producing damages and sometimes casualties. For this reason, hydrogeological risk reduction is crucial. Mitigation strategies aim to reduce hydrogeological risk to an acceptable level and can be classified into structural and non-structural measures. This work focuses on enhancing some non-structural risk mitigation measures for mountain areas: debris-flow rainfall thresholds, as a part of an Early Warning System (EWS), multivariate rainfall scenarios with multi-hazard mapping purpose and public awareness. Regarding debris-flow rainfall thresholds, an innovative calibration method, a suitable uncertainty analysis and a proper validation process are developed. The Backward Dynamical Approach (BDA), a physical-based calibration method, is introduced and a threshold is obtained for a study area. The BDA robustness is then tested by assessing the uncertainty in the threshold estimate. Finally, the calibrated threshold's reliability and its possible forecast use are assessed using a proper validation process. The findings set the stage for using the BDA approach to calibrate debris-flow rainfall thresholds usable in operational EWS. Regarding hazard mapping, a multivariate statistical model is developed to construct multivariate rainfall scenarios with a multi-hazards mapping purpose. A confluence between a debris-flow-prone creek and a flood-prone river is considered. The multivariate statistical model is built by combining the Simplified Metastatistical Extreme Value approach and a copula approach. The obtained rainfall scenarios are promising to be used to build multi-hazard maps. Finally, the public awareness within the LIFE FRANCA (Flood Risk ANticipation and Communication in the Alps) European project is briefly considered. The project action considered in this work focuses on training and communication activities aimed at providing a multidisciplinary view of hydrogeological risk through the holding of courses and seminars.

Marta Martinengo is an Environmental Engineer. She earned a Bachelor's degree in Environmental Engineering in 2014 frrom the University of Brescia and a Master's degree in Environental Engineering in 2017 from the University of Trento with a specialization in land defence and civil protection. In 2017 Marta Martinengo started her PhD research at the Department of Civil, Environmental and Mechanical Engineering of the University of Trento. Her research concerned some non-structural strategies of mitigation of the hydrogeological risk.